This is a repository copy of *Study of intercooling for rotating packed bed absorbers in intensified solvent-based CO2 capture process*.

White Rose Research Online URL for this paper:
http://eprints.whiterose.ac.uk/132997/

Version: Accepted Version

Article:

Study of intercooling for rotating packed bed absorbers in intensified solvent-based CO$_2$ capture process

Eni Oko, Colin Ramshaw and Meihong Wang[*]

Department of Chemical and Biological Engineering, University of Sheffield, S1 3JD, UK

*Corresponding Author: Tel.: +44 11142227160. E-mail address: Meihong.Wang@sheffield.ac.uk

Abstract

Rotating packed beds (RPBs) are a compact and potentially more cost-effective alternative to packed beds for application in solvent-based carbon capture process. However, with concentrated monoethanolamine (MEA) (up to 70-80 wt %) as the solvent, there is a question as to whether intercooler is needed for the RPB absorbers and how to design and operate them. This study indicates that the liquid phase temperature could rise significantly and this makes it essential for RPB absorber to have intercoolers. This is further assessed using a validated RPB absorber model implemented in gPROMS ModelBuilder® by evaluating the impact of temperature on absorption performance. Different design options for RPB absorber intercoolers (stationary vs rotary) were introduced and their potential sizes and associated pressure drop were evaluated based on a large scale flue gas benchmark of a 250 MWe Natural Gas Combined Cycle Power Plant. This paper addresses a fundamental question about intercooling in RPB absorber and introduces strategies for the intercooler design.

Keywords: solvent-based CO$_2$ capture, process intensification, rotating packed bed, absorber intercooling

Nomenclature

a	Effective interfacial area of packing per unit volume (m^2/m^3)
a_t	Total area of packing per unit volume (m^2/m^3)
a_p^i	Surface area of the 2 mm diameter bead per unit volume of the bead (1/m)
A	Tangential section area (m^2) = $2\pi r Z$; Heat exchanger area (m^2)
$C_{p,soln}$	Specific heat capacity of MEA solution (kJ/kg K)
C_p	Specific heat capacity (J/kg K)
d_i	Tube inside diameter (m)
d_o	Tube outside diameter (m)
d_e	Hydraulic diameter (m)
d_h	Hydraulic diameter (m) = $4\epsilon/a_t$
d_p	Effective diameter of packing (m) = $6(1-\epsilon)/a_t$
$D_{G,i}$	Gas diffusivity of component i (m^2/s)
$D_{L,i}$	Liquid diffusivity of component i (m^2/s)
E	Enhancement factor

F_t	Log-mean temperature correction factor
G	Volumetric gas flowrate (m³/s)
G^m	Gas molar flowrate (kmol/s)
h_G	Gas phase specific molar enthalpy (J/kmol)
h_L	Liquid phase specific molar enthalpy (J/kmol)
$h_{g/l}$	Interfacial heat transfer coefficient (W/m² K)
h_{sol}	Heat transfer coefficient for solvent side (W/m² K)
h_w	Heat transfer coefficient for cooling water side (W/m² K)
H	Henry constant (Pa m³/mol)
ΔH_r	Heat of absorption (kJ/mol CO_2)
ΔH_{vap}	Heat of vaporisation of H_2O (J/kmol)
k_f	Thermal conductivity of MEA solution/cooling water (W/m K)
k_{app}	Apparent reaction rate constant (1/s)
$k_{g,i}$	Mass transfer coefficient of gas for component i (m/s)
$K_{tot,i}$	Overall mass transfer coefficient of gas for component i (mol/(m².Pa.s))
$k_{l,i}$	Mass transfer coefficient of liquid for component i (m/s)
L^m	Liquid molar flowrate (kmol/s)
L_m^*	Liquid mass flowrate per unit tangential section area (kg/m² s)
L_P	Path length (m)
m_{CO_2}	molar flow of CO_2 entering absorber (kmol/s)
$\dot{m}_{CW}$	Cooling water flowrate (kg/s)
$\dot{m}_{fg}$	Molar flowrate of flue gas (kmol/h)
$\dot{m}_{sol}$	Solvent flowrate (kg/s)
M_{MEA}	Molar mass of MEA (kg/kmol)
$[MEA]$	MEA solution concentration (mol/L)
N_i	Component molar fluxes (mol/m² s)
p_{CO_2}	Equilibrium partial pressure of CO_2 (kPa)
$P_{g,i}$	Gas phase partial pressure of component i (Pa)
P_i^*	Equilibrium partial pressure of component i (Pa)
Pr	Prandtl Number
Q	Intercooler duty (W)
r	Radius (m)
r_i	Inner radius of the packed bed (m)
r_o	Outer radius of the packed bed (m)
r_s	Radius of the stationary housing (m)
R	Ideal gas constant (J/K mol)
Re	Reynolds number
R_t	Parameter for calculating F_t for shell and tube heat exchanger
S_t	Parameter for calculating F_t for shell and tube heat exchanger
T	Temperature (K)
T_g, T_l	Gas and liquid side temperature (K)
$T_{soln,IN}$	Solvent temperature at inlet intercooler (K)
$T_{soln,OUT}$	Solvent temperature at outlet of intercooler (K)
W_{MEA}	MEA concentration (wt %)

u_L	Liquid velocity (m/s)
u_P	Channel velocity for plate exchanger (m/s)
U	Overall heat transfer coefficient (W/m^2 K)
V_G	Parameter for Chen et al. (2011) gas film model = $1 - 0.9\frac{V_o}{V_t}$
V_m^*	Gas mass flowrate per unit tangential section area (kg/m^2 s)
V_O	Volume between the outer radius of the bed and the stationary housing (m^3) = $\pi(r_s^2 - r_o^2)Z$
V_t	Total volume of the RPB (m^3) = $\pi r_s^2 Z$
x_i	Component molar fraction in liquid phase
y_i	Component molar fraction in gas phase
Z	Height of the rotor (m)

Greek Letters

α_{lean}	Lean loading (mol CO_2/mol MEA)
α_{rich}	Rich loading (mol CO_2/mol MEA
$\Delta\alpha$	α_{rich} - α_{lean}
ρ_{soln}	Density of MEA solution (kg/L)
ΔP	Pressure drop (N/m^2)
ΔT_{lm}	Log mean temperature difference (K)
μ	Viscosity (Pa.s)
σ_c	Critical surface tension for packing material (N/m)
σ_L	Liquid surface tension (N/m)
ε	Packing porosity (m^3/m^3)
ρ_G	Gas density (kg/m^3)
ρ_L	Liquid density (kg/m^3)
λ_L	Liquid thermal conductivity (W/m K)
μ_G	Gas dynamic viscosity (Pa s)
μ_L	Liquid dynamic viscosity (Pa s)
ω	Rotating speed (rad/s)

Abbreviations

CCS/CCU	Carbon capture and storage/utilization
FG	Flue gas
ICAE	International Conference on Applied Energy
ITC	International Test Centre
MDEA	Methyl diethanolamine
NGCC	Natural Gas Combined Cycle
PB	Packed bed
PCC	Post-combustion CO_2 capture
PI	Process intensification
RPB	Rotating packed bed
RPM	Revolutions per minute

1. Introduction

1.1 Background

3

CCS/CCU technology is a significant climate change mitigation technology [1]. It is considered to be vital for economically and sustainably reaching long-term mitigation targets [2, 3]. The PCC process is the most matured and commercially ready approach for deploying CCS/CCU [4-5]. However, a major drawback of the PCC process is that PBs used as absorbers and strippers in the process are large, and this contributes significantly to plant footprint, capital, and operating costs [7]. PI technologies such as RPBs are considered to have an excellent potential to reduce the column sizes and consequently the cost and footprint of the entire PCC plant [8]. RPBs have been investigated in this regard in the literature [9-12]. These studies confirmed the potential for significant reduction in size with RPB as predicted in an earlier study by Ramshaw and Mallinson [9]. A report by HiGee Environment & Energy Technologies Inc., a PI company based in Pittsburgh USA, showed that between 1999 and 2011 about thirty-six commercial scale RPB units were installed mainly in China and other places around the world for different applications [13]. One of the installed RPBs, owned by Fujian Refining & Petrochemical Company Ltd, used for co-absorption of H_2S and CO_2 using MDEA solvent is about ten times smaller in size compared to the PB it replaced [13].

1.2   Operating principle of RPB

The RPB absorber comprises annular packed bed (rotor) mounted on a rotating shaft with the gas and liquid phases flowing counter-currently (or co-currently) in the radial direction across the bed (Fig.1) [14]. The liquid and gas phases are subjected to intense centrifugal acceleration which is many times the gravitational acceleration in PBs. The presence of centrifugal acceleration enhances mass transfer, which occurs both in the bed and the area between the packing and the casing [15-16], and extends the flooding limits. This is the reason for the drastic reduction in packing volume in RPBs. The bed is made of packing materials which could be wire mesh [17], expamet [18] or beads [19] among others.
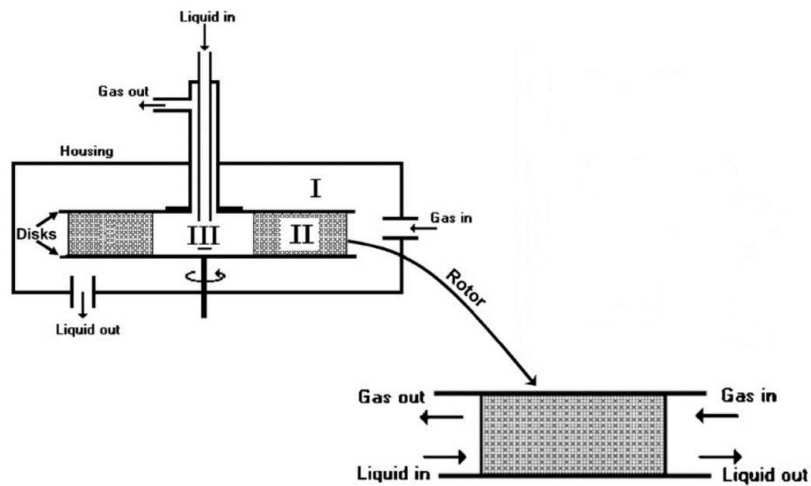
Fig. 1 Sectional view of an RPB [20]

1.3 Problem statement

In PBs with 30 wt% MEA solution as solvent, liquid phase temperature rise in the absorber has been identified and the effects on overall performance studied extensively [21-23]. The earlier study by Freguia and Rochelle [21] showed that the liquid phase temperature could rise by about 20-35°C depending on the gas phase CO_2 concentration (Fig. 2). Freguia and Rochelle [21] also showed that by intercooling the liquid phase in PBs, the overall absorption performance could improve by up to 10%.

The results were corroborated in later studies by Kvamsdal and Rochelle [22] and Biliyok et al. [23]. Following the outcome of these investigations, current commercial PCC designs include an absorber intercooler [24] which are typically shell and tube heat exchanger designs.

The short version of the paper was presented at ICAE2017, Aug 21-24, Cardiff, UK. This paper is a substantial extension of the short version of the conference paper.
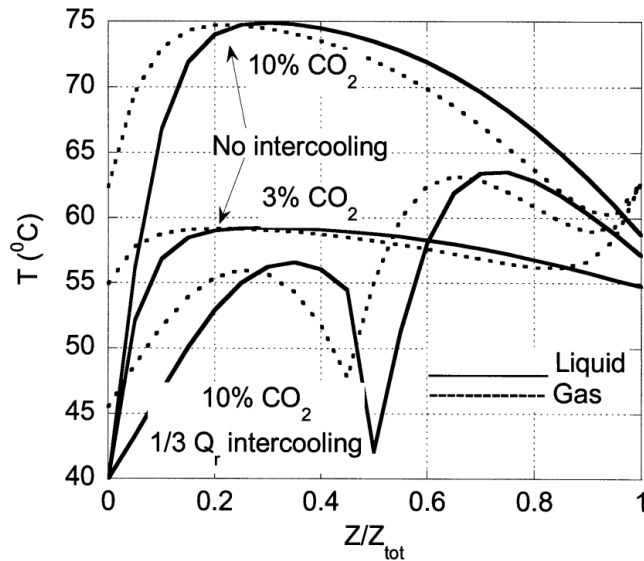
Fig. 2 PB absorber profile using 30 wt% MEA solvent [21]

In contrast, in centrifugal contactors such as RPBs, stronger MEA solutions, up to 100 wt% in some studies [25], is preferred as the benchmark solvent. Kang et al. [10] demonstrated that the liquid phase temperature could rise by about about 10-15°C in RPBs using 30 wt% MEA solution as solvent leading to a temperature bulge. However, the RPB absorber size of 16 mm outside diameter and differential CO_2 loading of about 0.04 are both small for signifcant temperature rise to be observed. For such a small RPB absorber, ongoing experiments with our collaborators at Newcastle University, UK show that most of the temperature rise occur in the rich solvent sump. This is due to the short residence time in the RPB absorber. The temperature rise could be higher with stronger MEA solution as solvent (> 30 wt%) and industrial size RPB absorber. Also, if the RPB absorber intercoolers are large like in PBs, the aim of physical size reduction with RPBs could be dealt a major blow. Investigations addressing these points namely temperature rise potentials in RPBs with strong MEA solution and their intercooler design are currently not reported in literature.

1.4   Case for concentrated MEA solution as solvent in RPBs

With 30 wt% MEA solvent, about 4 μm/year corrosion rate is predicted in PB absorbers at about 50°C according to tests conducted at ITC, Canada [26]. The corrosion rate will become significant with more concentrated MEA solution; visible corrosion level has been reported in a mild steel RPB rig using 100 wt% MEA as solvent [25]. More concentrated MEA solutions are also very viscous, for instance, the viscosity of a 70 wt% MEA solution is about 4-5 times

6

(depending on the CO_2 loading) that of a 30 wt% MEA solution according to data from Aspen Plus®. Higher viscosity reduces wetting potential of the packing and consequently slows down mass transfer. Due to these characteristics, concentrated MEA solutions (> 30 wt %) are generally perceived to be unsuitable as solvent in PB absorbers for CO_2 capture. However, with concentrated MEA solutions, CO_2-MEA reaction will be more rapid [27] and this is an important characteristic required of solvents in RPBs due to the smaller packing volume. This enhances the driving potential for mass transfer. The enhanced acceleration environment also enables RPBs to generally tolerate viscous solvents and as such they handle viscous solvents such as concentrated MEA solutions (> 30% wt MEA) efficiently [18]. The solvent flowrate as shown in Section 4 of this paper also decreases with increasing solvent concentration. The reboiler duty for the complete RPB-based PCC process estimated according to the approach of Oexmann [28] is about 3.10 and 2.94 GJ/ton CO_2 for 70 and 80 wt% MEA solvent respectively compared to about 4.00 GJ/ton CO_2 for 30 wt% MEA solvent [29]. The lower reboiler duty is due to the lower heat capacity and water fraction of the concentrated MEA solution. With these benefits in mind, RPBs are generally made with stainless steel (or other corrosion-resistant materials) to deal with the high corrosive effect of concentrated MEA solvent [18]. The smaller packing volume makes this economically feasible. An economic analysis conducted by Joel [30] showed that the total cost of RPB-based solvent CO_2 capture (with the RPBs made of stainless steel) from a 400 MWe NGCC power plant is about €61/tCO_2 compared to about €65/tCO_2 for the packed bed-based technology for the same power plant as reported by Agbonghae et al. [31].

1.5 Aim and objectives

The aim of this paper is to answer a key question whether it is necessary to have intercooling when high concentration MEA is used as solvent in RPB absorber for CO_2 capture. This is determined by analyzing the accompanying temperature rise for different MEA concentrations and also using a validated steady state RPB absorber model developed in this study to analyse the impact of temperature on parameters that relate to the absorption performance, namely liquid phase speciation, equilibrium partial pressure and mass transfer resistance. Joel et al. [9] and Kang et al. [10] analyzed temperature profile for RPBs with strong MEA solution as solvent. However, the analysis by Joel et al. [9] based on Jassim et al. [18] benchmark involved only a small fraction of CO_2 absorption in a tiny RPB rig of

about 398 mm diameter and did not as a result reveal temperature rise potentials. Another analysis by Kang et al. [10] based on Yu et al. [32] benchmark showed temperature rise potentials of about 10-15°C. However, this was performed using 30 wt% MEA solution as solvent. In this study, energy balance calculations are used to estimate accompanying temperature rise for different MEA concentrations and model-based analysis to determine the impact of temperature on parameters that relate to the absorption performance. Intercooler design options, namely stationary and rotary intercoolers are introduced and the potential intercooler sizes for different cases evaluated. The pressure drops associated with the stationary design (i.e. shell and tube and plate heat exchanger) are also investigated.

1.6   Novelty

The analysis on potential temperature increase described in Section 2, which demonstrated potential liquid phase temperature rise of about 40-80°C for CO_2 absorption in MEA depending on the concentrations of the MEA solution and the differential loading of CO_2, was presented at the ICAE 2017 [33]. The study has been extended by assessing the impact of temperature on parameters that relate to the absorption performance, namely liquid phase speciation, equilibrium partial pressure and mass transfer resistance using a validated RPB absorber model implemented in gPROMS ModelBuilder$^{®}$. Extensive physical property regression was performed in developing the RPB absorber model to ensure reliable estimates of the physical properties of the concentrated MEA solution. Existing RPB absorber models reported in [9-12] were developed using default physical property correlations for 30 wt% MEA solution. In addition, different intercooler design concepts – stationary and rotary – were compared and their potential sizes and associated pressure drop were evaluated based on a large scale flue gas benchmark of a 250 MWe Natural Gas Combined Cycle Power Plant. The stationary intercooler follows from the same concept as intercoolers in PBs where they are located at a suitable position (pinch point) along the column height which typically divides the column into an upper section (above the intercooler) and a lower section (below the intercooler). For RPBs, both sections are represented by two separate RPB absorbers with the intercooler between them (Fig.19). On the other hand, the rotary intercooler which is incorporated within the RPB rotor is a new design not reported previously in literature. With these analyses, this paper addresses two important fundamental questions: (i) the need for intercoolers for RPB absorbers operating with concentrated MEA solution as solvent and (ii)

8

2. Estimation of temperature rise for different MEA concentrations

The temperature rise (ΔT) for CO_2 absorption in a given concentration of MEA solution is estimated using Eqn 1. The ΔH_r is obtained by applying the Gibbs-Helmholtz equation to solubility data [34] as existing experimental data of ΔH_r in literature obtained from direct calorimetric measurements are mainly for 30 wt% MEA solution. The only existing data of ΔH_r for higher concentration is for 70 wt% MEA solution at 120°C [35]. The Gibbs-Helmholtz equation is given in Eqn 2.

$$\Delta T = \frac{\Delta H_r (\alpha_{rich} - \alpha_{lean})[MEA]}{\rho_{soln} C_{p,soln}} \tag{1}$$

$$\left[\frac{\partial \ln p_{CO_2}}{\partial \left(\frac{1}{T} \right)} \right]_p = \frac{\Delta H_r}{R} \tag{2}$$

The solubility data is obtained using Electrolyte Non-Random-Two-Liquid (eNRTL) activity coefficient model in Aspen Plus®. The default eNRTL model parameters have been updated for concentrated MEA solution (> 30 wt%) using solubility data from literature [36-37] via Aspen Plus® Data Regression System. Comparison between the regressed eNRTL model predictions and the experimental data show reasonable agreement for different MEA concentrations (Figs. 3-5).
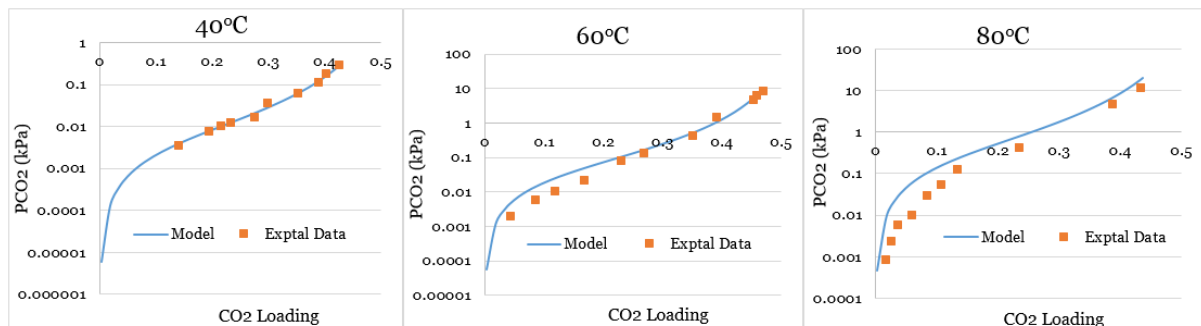

Fig. 3 Model prediction for 45 wt% MEA solution with data from Aronu et al. [36]
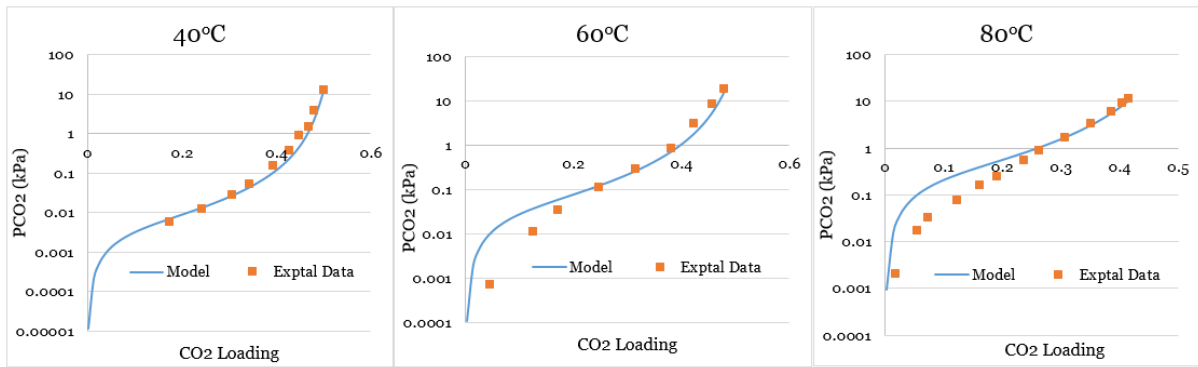
9

Fig. 4 Model prediction for 60 wt% MEA solution with data from Aronu et al. [36]
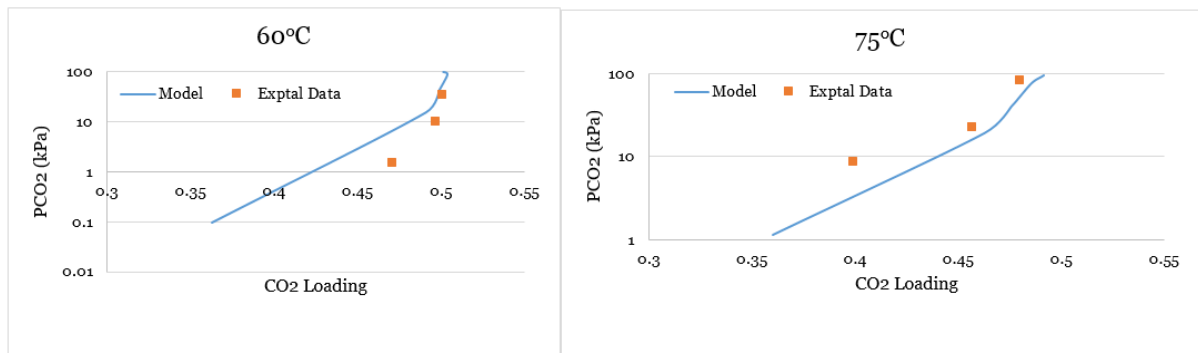

Fig. 5 Model prediction for 75 wt% MEA solution with data from Mason and Dodge [37]

Generally, Gibbs-Helmholtz equation is inherently inaccurate for estimating ΔH_r due to the accompanying numerical differentiation [38]. The prediction error is expected to be as high as $\pm 20\%$ [39]. From our comparison of the predicted ΔH_r for CO_2 absorption in 30 wt% MEA at 40°C with experimental data [35], it can be seen that the prediction error is about 10% (Fig. 6). This is reasonable considering both errors in the solubility data and ΔH_r predictions. The prediction errors were also found to be slightly higher for higher concentration when compared to 70 wt% MEA data [35]. The data for 70 wt% MEA was taken at 120°C and it is the only data for MEA concentrations higher than 30 wt% [35]. Nevertheless, the trend of ΔH_r is similar for different concentrations compared to the reported trends for 30 and 70 wt% MEA as shown in Fig. 7. The results in Fig. 7 show that ΔH_r increases slightly with concentration and the ΔH_r for any concentration is also relatively constant up to about a loading of 0.45 mol CO_2/mol MEA. The decline in ΔH_r beyond loading of about 0.45 reflects onset of saturation as less CO_2 is absorbed. The upper limit loading range in the RPB is expected to be about 0.45 mol CO_2/mol MEA. On this basis, it is

The short version of the paper was presented at ICAE2017, Aug 21-24, Cardiff, UK. This paper is a substantial extension of the short version of the conference paper.

therefore safe to assume that ΔH_r is fixed over the operating loading range in RPBs for different MEA concentrations.
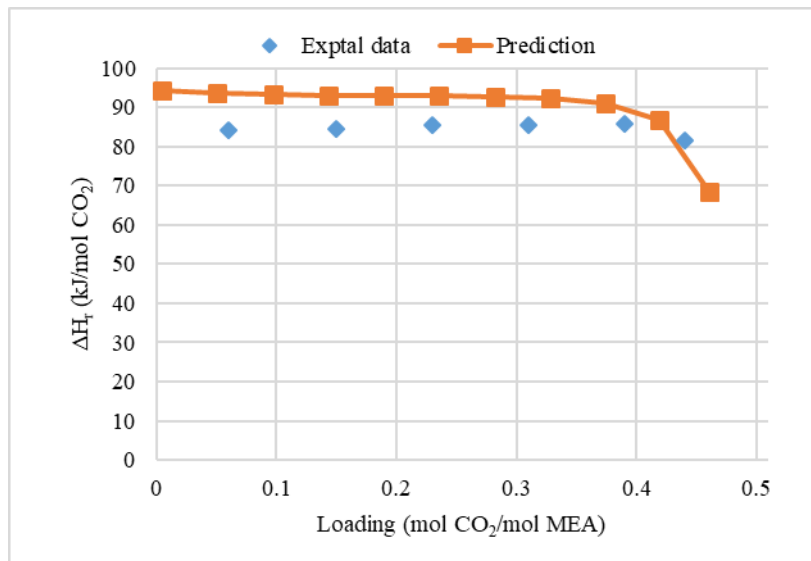

Fig. 6 Predicted data vs experimental data for 30 wt% MEA solution
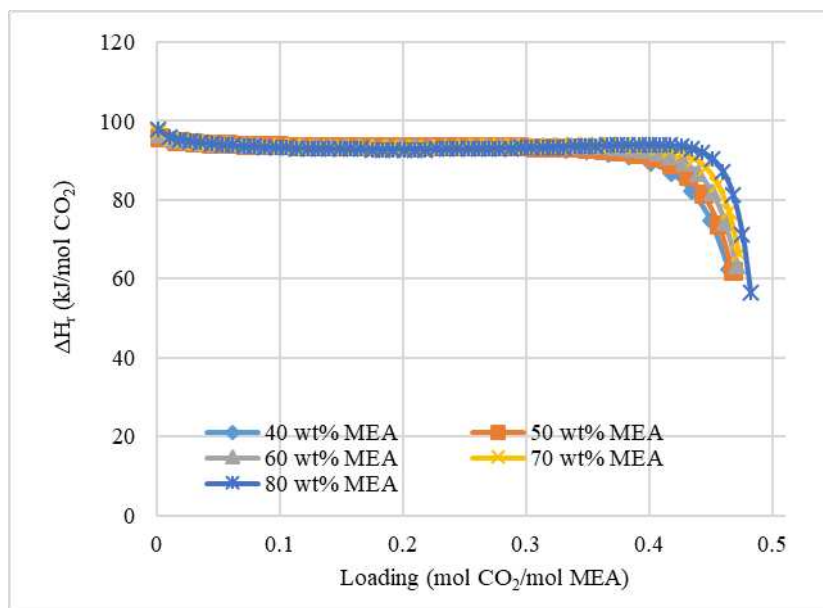
Fig. 7 Predicted ΔH for different MEA concentrations

Based on the predicted ΔH_r values and other parameters shown in Table 1 (the density and specific heat capacity have been obtained from Aspen Plus® database), the ΔT is estimated for different MEA concentrations using Eqn. 1. Three hypothetic scenarios involving differential loadings (i.e. α_{rich} - α_{lean}) of 0.15, 0.20 and 0.25 have been assumed. These

The short version of the paper was presented at ICAE2017, Aug 21-24, Cardiff, UK. This paper is a substantial extension of the short version of the conference paper.

differential loadings are generally achievable based on experience from PBs using 30 wt% MEA solution as solvent with initial loading of about 0.20.

Table 1. Input conditions used for ΔT estimation

W_{MEA} (wt %)	ρ_{soln} (kg/L)	$[MEA]$ (mol/L)	$C_{p,soln}$ (kJ/kg K)	$\alpha_{rich} - \alpha_{lean}$
40	1.144	6.6	3.069	
50	1.186	8.2	2.874	0.15,0.2,0.25
60	1.228	9.8	2.685	
70	1.273	11.5	2.477	

The results in Fig. 8 show increase in ΔT as concentration increases. This is attributed to the following:

- Heat of absorption: Increase in temperature rise as concentration increased was because the heat of absorption for more concentrated solutions are slightly higher as demonstrated in Fig.7.

- Specific heat capacity: The specific heat capacity of the solution decreases as concentration increases (Table 1). This means that any given amount of heat in the solution, will potentially result in higher ΔT in more concentrated solutions than in less concentrated solution.

The ΔT is also higher as differential loading ($\Delta\alpha$) increases. For a fixed initial loading (in this analysis initial loading of 0.20 mol CO_2/mol MEA was assumed for all the cases), increasing differential loading means that more CO_2 is absorbed and invariably more heat is released during CO_2-MEA reaction. Water vaporization and the packings are expected to have some cooling effect on the solution [10] and as such estimated ΔT using the method in this study will be slightly higher than actual ΔT. However, in RPBs the smaller packing volume and the higher concentration of the solvent mean that that the potential cooling effect will be less in RPBs. The estimated ΔT will therefore not be far away as such from the actual ΔT.
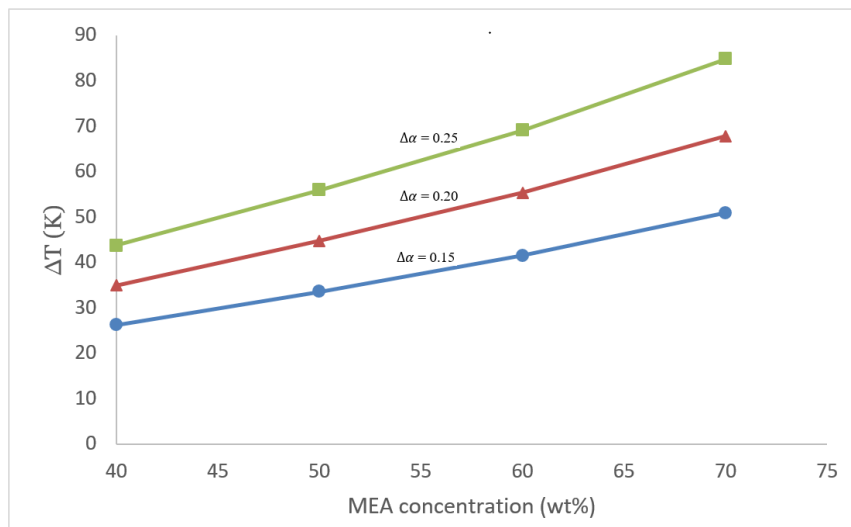
Fig.8. Estimated temperature rise for different scenario

3. RPB absorber model

The analysis in Section 2 showed potential temperature rise for CO_2 absorption under different MEA concentrations. In this section, additional evidence regarding the impact of temperature on liquid phase speciation, equilibrium partial pressure and mass transfer resistance, are presented. To carry out this analysis, a steady state first principle model of an RPB absorber implemented in gPROMS Model Builder® was developed. The developed model was validated against experimental data to demonstrate the model fidelity.

3.1 Model development

The assumptions made in deriving the model equations include:

- Steady state conditions

- One-dimensional differential mass and energy balances for liquid and gas phases

- Heat losses are neglected

- Reactions are assumed to occur in the liquid film and this is taken into account using an enhancement factor in the overall mass transfer coefficient

3.1.1 Model Equations

Based on the assumptions, the model is derived using the following equations.

<u>Mass balance:</u>

Gas phase:
$$0 = \frac{1}{2\pi r Z}\frac{\partial(G^m y_i)}{\partial r} - aN_i \tag{3}$$

Liquid phase:
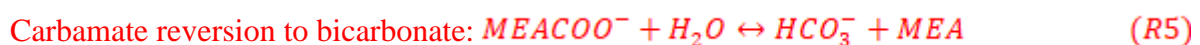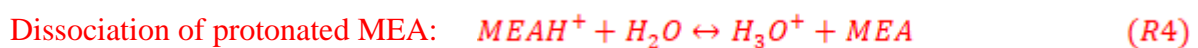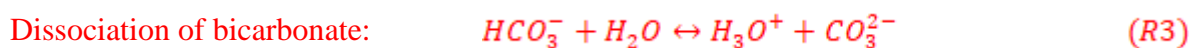$$0 = -\frac{1}{2\pi r Z}\frac{\partial(L^m x_i)}{\partial r} + aN_i \tag{4}$$

<u>Energy balance:</u>
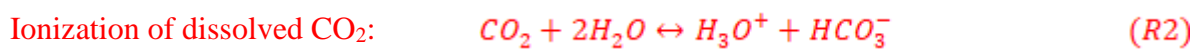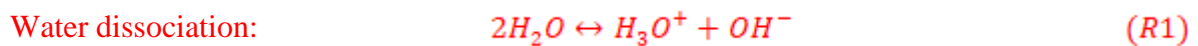
Gas phase:
$$0 = \frac{1}{2\pi r Z}\frac{\partial(G^m h_G)}{\partial r} - ah_{g/l}(T_l - T_g) \tag{5}$$

Liquid phase:
$$0 = -\frac{1}{2\pi r Z}\frac{\partial(L^m h_L)}{\partial r} + a\left(h_{g/l}(T_l - T_g) - \Delta H_r N_{CO_2} - \Delta H_{vap} N_{H_2O}\right) \tag{6}$$

The unit of ΔH_r in Eqn 5 is J/kmol.

3.1.2 Thermo-physical model

The vapour-liquid equilibrium, chemical equilibrium and physical properties are described based on the eNRTL property method in Aspen Plus®. The eNRTL property method is accessed from gPROMS ModelBuilder® via the CAPE-OPEN interface. The default eNRTL activity coefficient model parameters were updated and validated for concentrated MEA solution as described in Section 2. The liquid phase speciation is described based on the following equilibrium chemical reactions with the equilibrium constant data obtained from Aboudheir et al. [40].

Water dissociation:
$$2H_2O \leftrightarrow H_3O^+ + OH^- \tag{R1}$$

Ionization of dissolved CO_2:
$$CO_2 + 2H_2O \leftrightarrow H_3O^+ + HCO_3^- \tag{R2}$$

Dissociation of bicarbonate:
$$HCO_3^- + H_2O \leftrightarrow H_3O^+ + CO_3^{2-} \tag{R3}$$

Dissociation of protonated MEA:
$$MEAH^+ + H_2O \leftrightarrow H_3O^+ + MEA \tag{R4}$$

Carbamate reversion to bicarbonate:
$$MEACOO^- + H_2O \leftrightarrow HCO_3^- + MEA \tag{R5}$$

The gas phase properties were obtained directly from Aspen Plus®. The sources of the liquid phase property predictions are summarised in Table 2. The regressed correlations namely, density and viscosity correlations agree well with experimental data as shown in Fig 9-10.

14

The short version of the paper was presented at ICAE2017, Aug 21-24, Cardiff, UK. This paper is a substantial extension of the short version of the conference paper.

The surface tension correlation based on default parameters in Aspen Plus® also showed good agreement in comparison to experimental data as shown in Fig 11.

Table 2. Liquid phase properties

| Property	Source	Note
Density	Aspen Plus®; Rackett equation [41]	Regression with experimental data [42] to obtain binary parameters for concentrated MEA
Viscosity	Aspen Plus®; Andrade equation with Jones-Dole correction for electrolyte [43]	Regression with experimental data [44] to obtain binary parameters for concentrated MEA
Surface tension	Aspen Plus®; Hakim-Steinberg-Stiel equation with Onsager-Samaras electrolyte correction [43]	Good agreement with concentrated MEA data [42]
Specific heat capacity	Agbonghae et al. [45] semi-empirical correlation	Developed based on data for concentrated MEA
Diffusivity	Ying and Eimer [46] correlation for CO_2; Diffusivity of other components obtained from Aspen Plus	Developed based on data for concentrated MEA
Henry constant	Ying et al. [47] correlation	Developed based on data for concentrated MEA
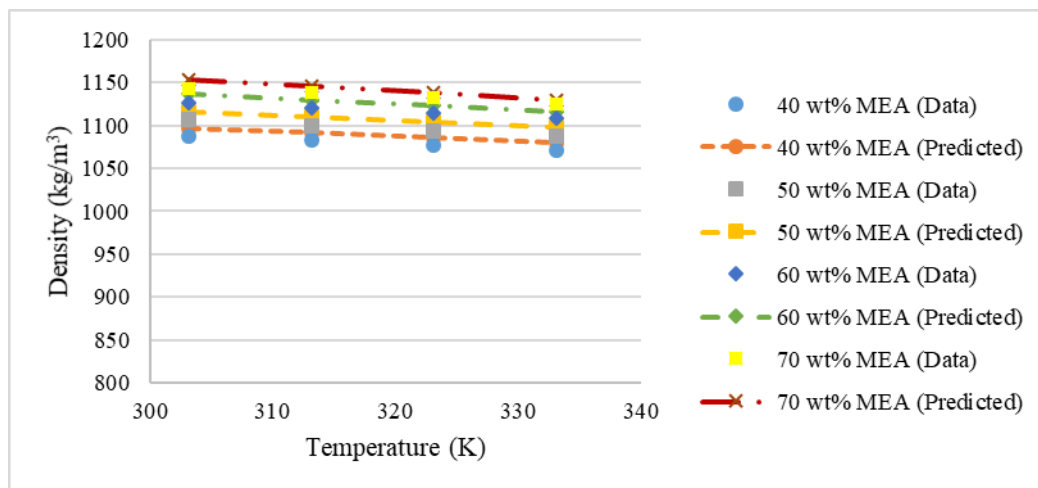
Fig.9. Liquid density correlation validation using Jayarathna et al. [42] data

15
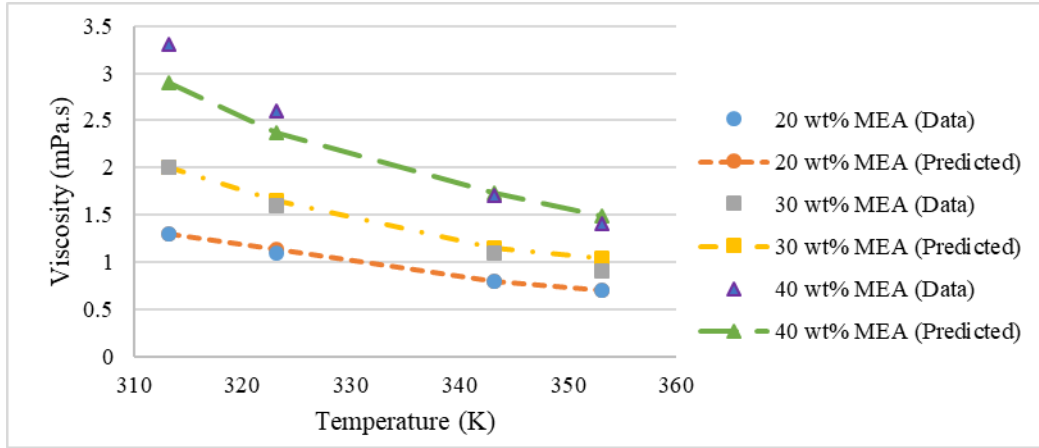
Fig.10. Liquid viscosity correlation validation using Amundsen et al. [44]
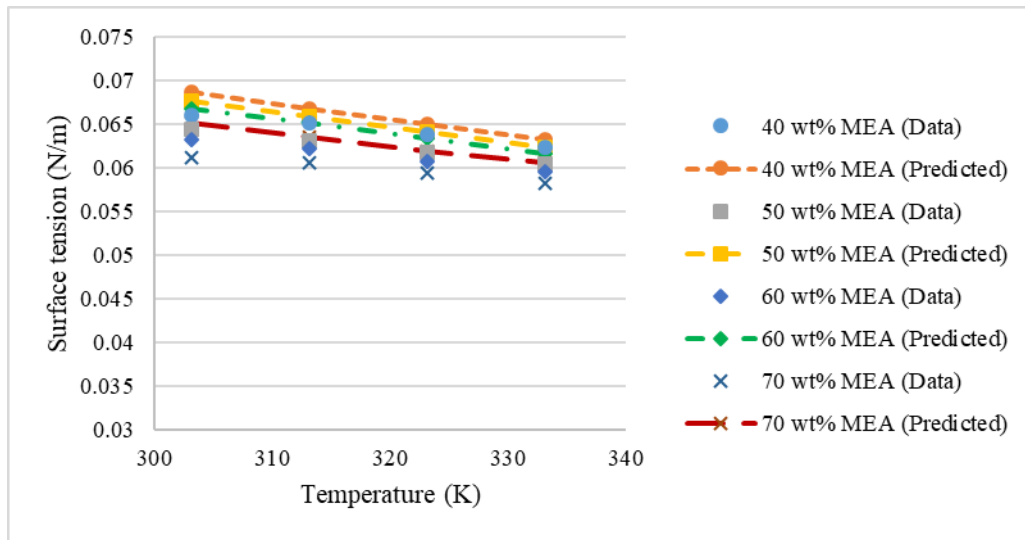
Fig.11. Surface tension correlation validation using Jayarathna et al. [42] data

3.1.3   Heat and mass transfers

The interfacial heat transfer coefficient $(h_{g/l})$ is obtained based on the Chilton-Colburn analogy [48]:

$$h_{g/l} = k_f \rho_L C_p^L \left(\frac{\lambda_L}{\rho_L C_p^L D_L} \right)^{\frac{2}{3}} \tag{7}$$

The mass transfer rate is modelled according to the two-film theory, wherein the molar fluxes for molecular components are obtained as follows [10]:

$$N_i = K_{tot,i} \left(P_{g,i} - P_i^* \right) \tag{8}$$

16

The short version of the paper was presented at ICAE2017, Aug 21-24, Cardiff, UK. This paper is a substantial extension of the short version of the conference paper.

The overall mass transfer coefficient ($K_{tot,i}$) for CO_2 is obtained by:

$$K_{tot,CO_2} = \frac{1}{\left(\frac{RT_g}{k_{G,CO_2}}\right) + \left(\frac{H}{k_{L,CO_2}E}\right)} \tag{9}$$

The $K_{tot,i}$ for other molecular components namely MEA, N_2, O_2 and H_2O is based on the gas film resistance only as shown in Eqn 10; the liquid side resistances are neglected. The ionic components are also assumed to exist in the liquid phase only and not transferred to the gas phase.

$$K_{tot,i} = \frac{k_{G,i}}{RT_g} \tag{10}$$

The equilibrium partial pressure (P_i^*) is called from Aspen Plus® in gPROMS Model Builder® using TPFlash method. The enhancement factor is estimated using Eqn 11 on the basis of pseudo first order reaction regime which is generally applicable for CO_2 absorption with MEA in packed columns [10, 49]. The apparent reaction rate constant (k_{app}) is obtained based on Aboudheir et al. [45] termolecular kinetics model which has been shown to be reliable for high MEA concentration in Kang et al. [10].

$$E = \frac{\sqrt{k_{app}D_{L,CO_2}}}{k_{L,CO_2}} \tag{11}$$

The effective interfacial area, liquid and gas film mass transfer coefficients were obtained using the following correlations. The choices are based on extensive comparison of different mass transfer correlations to experimental data [14].

Effective interfacial area [50]:

$$\frac{a}{a_t} = 1.5(a_t d_h)^{-0.5} \left(\frac{\rho_L u_L d_h}{\mu_L}\right)^{-0.2} \left(\frac{\rho_L u_L^2 d_h}{\sigma_L}\right)^{0.75} \left(\frac{u_L^2}{r\omega^2 d_h}\right)^{-0.45} \tag{12}$$

Liquid side mass transfer coefficient [51]:

$$\frac{k_{L,i}d_p}{D_{L,i}} = 0.918 \left(\frac{\mu_L}{D_{L,i}\rho_L}\right)^{\frac{1}{2}} \left(\frac{L_m^*}{\mu_L a_t}\right)^{\frac{1}{3}} \left(\frac{a_t}{a}\right)^{\frac{1}{3}} \left(\frac{d_p^3 \rho_L^2 r\omega^2}{\mu_L^2}\right)^{\frac{1}{6}} \tag{13}$$

Gas side mass transfer coefficient [52]:

$$\frac{k_{G,i}a}{D_{G,i}a_t^2}V_G = 0.023\left(\frac{V_m^*}{\mu_G a_t}\right)^{1.13}\left(\frac{L_m^*}{\mu_L a_t}\right)^{0.14}\left(\frac{d_p^3\rho_G^2 r\omega^2}{\mu_G^2}\right)^{0.31}\left(\frac{L_m^{2*}}{\sigma_L\rho_L a_t}\right)^{0.07}\left(\frac{a_t}{a_p^i}\right)^{1.4} \tag{14}$$

3.1.4 Gas phase pressure drop

The gas phase pressure drop (dry) is obtained using the correlation proposed by Llerena-Chavez and Larachi [20]:

$$\Delta P = \frac{150(1-\varepsilon)^2\mu_G}{d_p^2\varepsilon^3}\left(\frac{G}{2\pi Z}\right)\ln\left(\frac{r_o}{r_i}\right) + \frac{1.75(1-\varepsilon)\rho_G}{d_p\varepsilon^3}\left(\frac{G}{2\pi Z}\right)^2\left(\frac{1}{r_i}-\frac{1}{r_o}\right) +$$

$$\frac{1}{2}\rho_G\omega^2(r_o^2-r_i^2) + \varepsilon\left(-0.08 - G + G^2(2000(RPM)^{1.22}+\omega^{1.22})\right) \tag{15}$$

3.2 Model validation

The model equations presented in Section 3.1 were implemented and solved in gPROMS Model Builder® using the experimental data of Jassim et al. [53] as benchmark. The RPB absorber of Jassim et al. [53] used expamet stainless steel mesh with total surface area of 2132 m^2/m^3 and porosity of 0.76 m^3/m^3. The inner and outer diameters of the rotor are 0.156 m and 0.396 m respectively and axial height of 0.025 m. Jassim et al. [53] experiments considered high concentration MEA (55 and 75 wt %) which is very useful for the discussions in this paper. The capture level and rich loadings predicted with the model were validated against the experimental data [53] for different input conditions. The capture level and loading are predicted using Eqn 16 and 17.

$$\text{Capture level} = \left(\frac{y_{CO_2,in}-y_{CO_2,out}}{y_{CO_2,in}}\right) \tag{16}$$

$$Loading = \frac{y_{CO_2}+y_{HCO_3^-}+y_{CO_3^{2-}}+y_{MEACOO^-}}{y_{MEA}+y_{MEACOO^-}+y_{MEA^+}} \tag{17}$$

The experimental data include four cases; Cases 1 and 2 for lower MEA concentrations (53-57 wt%) and Cases 3 and 4 for higher MEA concentrations (72-78 wt%). Each case includes four runs with different rotational speed, lean temperature and lean loading. The gas phase for all the cases in the Jassim et al. [53] experimental work used for validating the model in this study is a CO_2/air mixture. The complete detail of the various cases is presented in Table 3.

The model validations for the different cases, presented in Fig. 12, showed relative deviation of about 0.3-3.0% for capture level and about 0.9-6.0% for rich loading. For all the cases, Runs 3 and 4 appeared to consistently give higher relative deviations than Runs 1 and 2. This could be because Billet and Schultes [50] correlation used to predict interfacial area in this study gives less accurate predictions at a higher RPM (Runs 3 and 4) than at lower RPM (Runs 1 and 2) [14]. The selection of Billet and Schultes [50] in this study was because as shown in Oko et al. [14], it gives more consistent and accurate prediction for RPBs compared to other correlations. With a relative deviation of about 0.3-6.0% for both capture level and rich loading prediction, the model in this study is considered robust and fit to be used to analyse the process to gain insight about different phenomena.

Table 3 Input process conditions for model validation [53]

| Cases	Runs	Rot. Speed (RPM)	Lean Temp. (K)	α_{lean}	Op. Press. (N/m²)	$\dot{m}_{sol}$ (kg/s)	$\dot{m}_{fg}$ (kmol/h)	CO₂ in FG (mol%)	Lean composition (wt%)		
									H₂O	MEA	CO₂
1	1	600	312.75	0.0772	101325	0.66	2.87	4.71	40.91	56.00	3.09
	2	600	293.85	0.0897	101325	0.66	2.87	4.60	43.35	53.20	3.45
	3	1000	313.25	0.0772	101325	0.66	2.87	4.48	40.91	56.00	3.09
	4	1000	294.05	0.0924	101325	0.66	2.87	4.45	42.40	54.00	3.60
2	1	600	312.65	0.1000	101325	0.35	2.87	4.43	41.01	55.00	3.99
	2	600	295.45	0.0955	101325	0.35	2.87	4.47	40.11	56.00	3.89
	3	1000	312.75	0.0996	101325	0.35	2.87	4.35	41.03	55.00	3.97
	4	1000	295.75	0.0945	101325	0.35	2.87	4.09	39.10	57.00	3.90
3	1	600	314.15	0.0492	101325	0.66	2.87	4.40	22.32	75.00	2.68
	2	600	294.55	0.0389	101325	0.66	2.87	4.36	20.83	77.00	2.17
	3	1000	313.35	0.0483	101325	0.66	2.87	4.36	23.41	74.00	2.59
	4	1000	293.85	0.0355	101325	0.66	2.87	4.29	23.00	75.10	1.90
4	1	600	313.95	0.0582	101325	0.35	2.87	3.55	24.95	72.00	3.05
	2	600	295.25	0.0443	101325	0.35	2.87	4.38	21.57	76.00	2.43
	3	1000	312.55	0.0523	101325	0.35	2.87	4.38	22.16	75.00	2.84
	4	1000	293.75	0.0407	101325	0.35	2.87	4.53	19.71	78.00	2.29
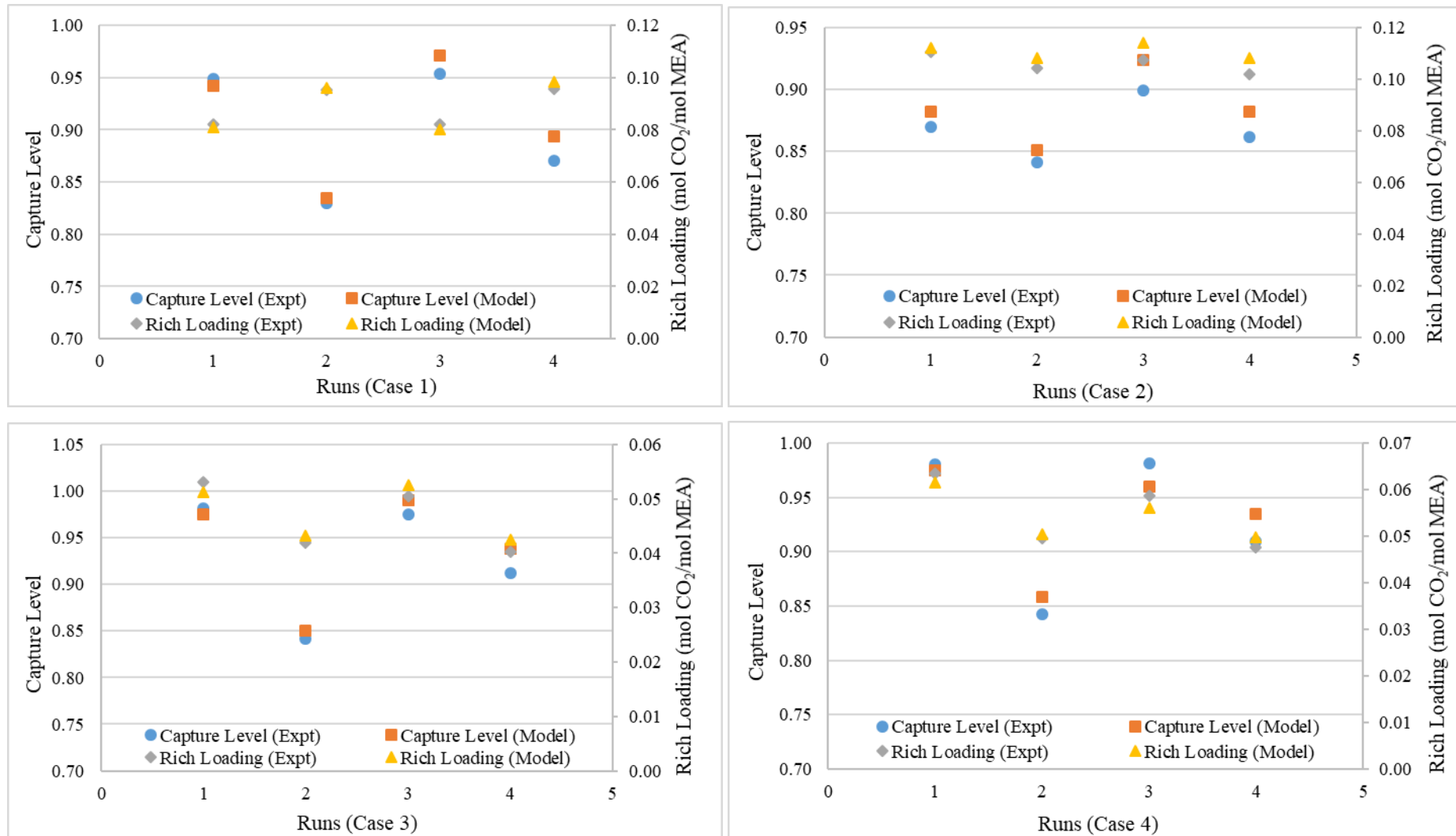
Fig. 12. Model validation results using Jassim et al. [53] experimental data

The short version of the paper was presented at ICAE2017, Aug 21-24, Cardiff, UK. This paper is a substantial extension of the short version of the conference paper.

3.3 Model analysis

3.3.1 Impact of temperature on liquid phase equilibrium composition

The equilibrium composition is the liquid bulk concentration for different components at any given temperature and CO_2 loading. The equilibrium composition for different temperatures will show the direction of equilibrium, whether to the product or reactant side. When the reaction is driven to the product side, more of the reacting MEA and CO_2 will be used up to form carbamates according to R5 and vice versa. Analysis of the impact of temperature on the equilibrium composition will therefore be a good way to demonstrate the impact of temperature on absorption performance.

The equilibrium composition in our model is based on mass balance of the liquid phase components and the chemical equilibrium constant [40]. The predicted equilibrium composition for different CO_2 loading using this method for 73.2 wt% MEA solution (Fig. 13) which although cannot be validated directly due to lack of data at this condition shows similar trends as the results from more complicated models for 30 wt% MEA solution [54-55]. The result shows that indeed the solution begins to saturate at about 0.45-0.5 CO_2 loading as less carbamates ($MEACOO^-$) are formed indicating that less CO_2-MEA reaction was taking place. This conclusion is in agreement with the deductions from Fig 7. The result also showed that below CO_2 loading of 0.5, CO_2 exists in the liquid phase in the form of $MEACOO^-$; concentration of free CO_2, CO_3^{2-} and HCO_3^- are neglible at this condition.

The impact of temperature on the concentration of $MEACOO^-$ is assessed for different CO_2 loading and MEA concentration (Fig. 14). The result shows that the MEACOO-concentration decreases as temperature increases. This shows that rising temperature drives the reaction equilibrium to the left (reactant side), wherein the products recombines to form the reacting species. This is a clear evidence that increase in temperature will limit absorption rate.
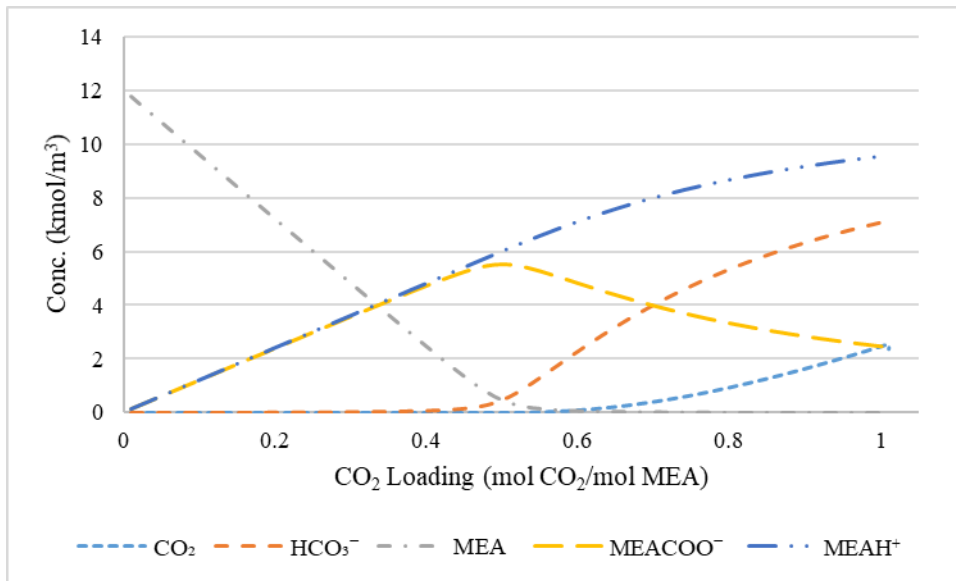
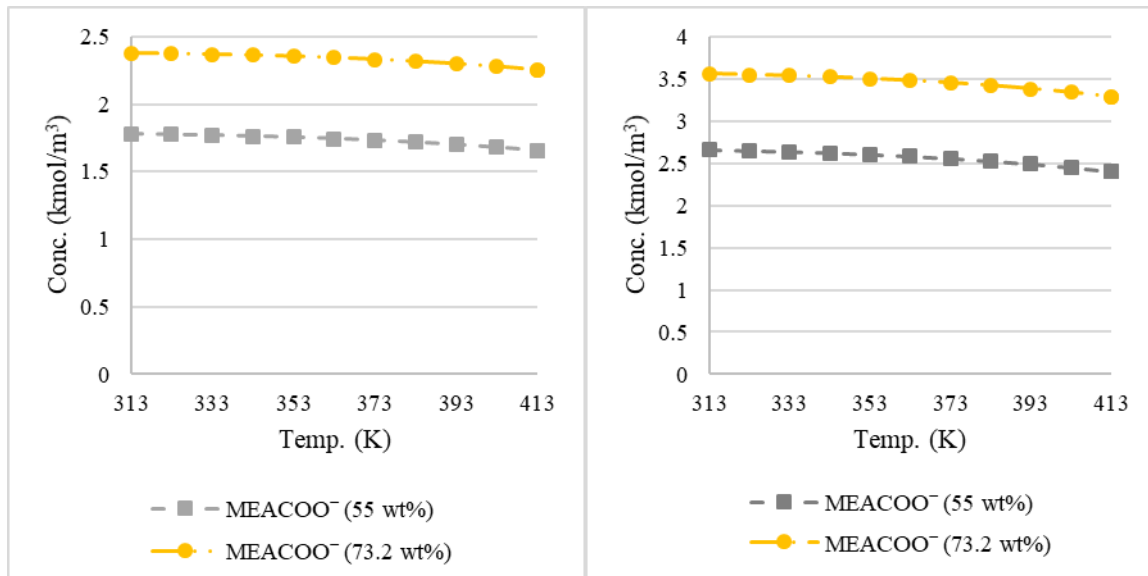Fig. 13. Liquid phase speciation (73.2 wt% MEA solution at 313 K)

Fig. 14. Liquid-phase concentration of carbamate (MEACOO⁻) for CO_2 loading of 0.2 (left) and 0.3 (right) for 55 and 73.2 wt% MEA solution

3.3.2   Impact of temperature on equilibrium partial pressure

The equilibrium partial pressure of (P_i^*) is an essential characteristic that contributes to the available gradient for mass transfer between the gas and liquid phase. As shown in Eqn 8, it directly affects the mass transfer rate between the gas and liquid phase and as such contributes to overall absorption performance. It is therefore important to show the impact of temperature on the equilibrium partial pressure. The impact of temperature on the equilibrium

22

partial pressure was predicted for different concentrations of an MEA solution (Fig 15) in terms of $P_{CO_2}^*$ following the descriptions in Section 3.1.2. The loading was fixed at approximately 0.3 mol CO_2/mol MEA and the total pressure fixed at 100 kPa for all the cases. The temperature was varied between 313 – 363 K as the temperature in the RPB is expected to vary between this ranges depending on the CO_2 loading.
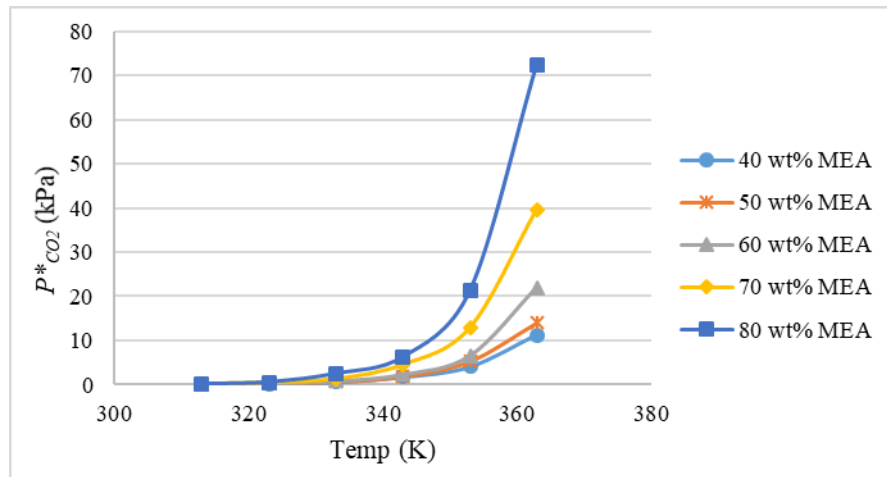

Fig. 15. Impact of temperature on equilibrium partial pressure of CO_2

The results in Fig. 15 showed that the equilibrium partial pressure increases significantly above temperature of 340 K. In addition, the increase rate of $P_{CO_2}^*$ above 340 K increases with the MEA wt%. The $P_{CO_2}^*$ depends on two parameters, namely the Henry constant and the concentration of free CO_2 in the liquid phase [10]. The Henry constant for any given concentration changes rather linearly with temperature [47] and do not explain the behaviour in Fig. 14 above 340 K. However, the concentration of free CO_2 in the liquid phase appears to follow a similar trend as Fig. 15 with temperature (Fig. 16) and could be largely responsible for the behaviour observed in Fig. 15. This further shows that as temperature increases up to a point that the reverse CO_2-MEA reaction begins to be favoured leading to increases in the concentration of free CO_2 in the liquid phase.

3.3.3   Impact of temperature on mass transfer resistance

The mass transfer resistance directly affects absorption rate as can be seen from Eqn 8 and how it changes with respect to temperature can give insight about the impact of temperature

on overall absorption performance. This makes it necessary for the impact of temperature on the mass transfer resistance to be investigated.
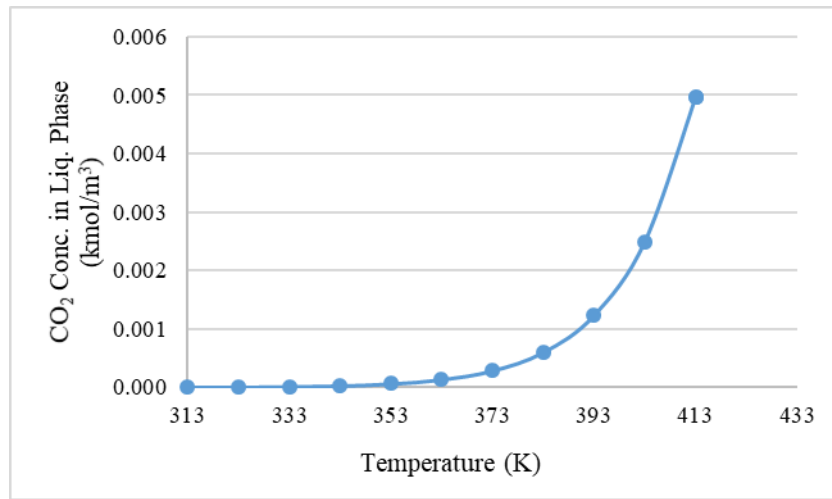

Fig. 16. CO_2 concentration in liquid phase for 55 wt% MEA at a loading of 0.2

The average mass transfer resistance across the RPB is obtained using the model developed in this study. Two cases involving 50 and 70 wt% as solvent was assessed to identify the impact of temperature on the mass transfer resistance for both cases. The rotor speed was maintained at 600 RPM for both cases and the lean solvent and gas flowrate maintained at 0.66 kg/s and 2.87 kmol/hr respectively. The gas inlet temperature was fixed at 300 K, while the lean inlet temperature was varied from 313-363 K. The lean loading was set at 0.08 and 0.05 mol CO_2/mol MEA for the 50 and 70 wt% MEA cases respectively. The lean loading and the total concentration is first applied to the liquid speciation model (Section 3.3.1) to determine the actual lean solvent composition (including the ionic components) which is then supplied to the RPB model.
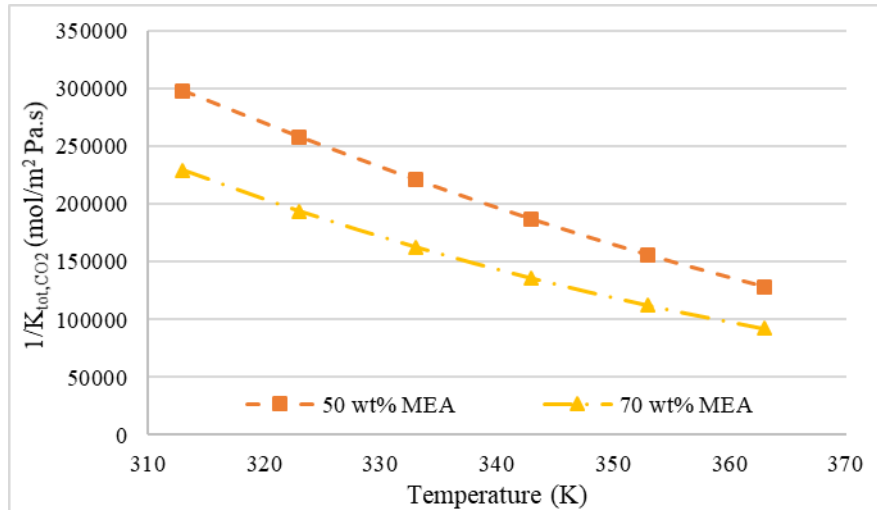
Fig. 17. Average mass transfer resistance for different temperature and MEA concentrations

The results presented in Fig. 17 show a good degree of mass transfer enhancement with respect to concentration and temperature. It should be noted that the mass transfer resistance depends on liquid and gas properties such as density, viscosity, diffusion coefficient, surface tension, physical solubility of the absorbed solute (in this case CO_2) in the solvent and more importantly the reaction kinetics. All these parameters are directly affected by temperature and concentration but it is the impact on reaction kinetics that have the greatest influence on the mass transfer resistance [27].

In summary, although temperature is seen to enhance mass transfer resistance from this analysis which is good for the absorption process, the results in Section 3.3.2 indicate potential tipping point above 340 K where increases in temperature could reduce available gradient for mass transfer due to its impact on the equilibrium partial pressure. In addition, as shown in Section 3.3.1, the reverse CO_2-MEA reaction may begin to dominate at certain temperature making chemical absorption by the solvent impossible. With the temperature rise predicted in Section 2, it is therefore imperative to intercool the solvent in RPBs to guarantee best performance.

4   RPB absorber intercooler design

4.1 Benchmark CO_2 source

Having established the necessity of intercooling in Sections 2 and 3, possible design approaches for RPB absorber intercoolers is introduced in this section including sizing and

25

pressure drop calculations. This is done using flue gas condition from a 250 MWe Natural Gas Combined Cycle (NGCC) power plant as benchmark. The flue gas specification for the power plant include flowrate of 356 kg/s and a composition of N_2 (86.2 wt%), H_2O (4.6 wt%), CO_2 (7.7 wt%) and Ar (1.5 wt%) [56]. The required solvent flowrate to treat the flue gas is estimated using the approach of Lawal et al. [57] presented in Eqn 18. The estimated solvent flowrate (Fig 18) reflects the impact of the solvent concentration and the differential loading ($\Delta\alpha$).

$$\dot{m}_{sol} = \frac{m_{CO_2} M_{MEA}}{\Delta\alpha W_{MEA}} \qquad (18)$$

4.2 Intercooler design options

4.2.1 Stationary intercooler design

The stationary intercooler is assumed to be deployed between two RPB absorbers as shown in Fig. 19 for cooling the liquid phase. Cooling the liquid phase removes more heat from the system than cooling the gas phase due to the higher density and heat capacity of the liquid phase.
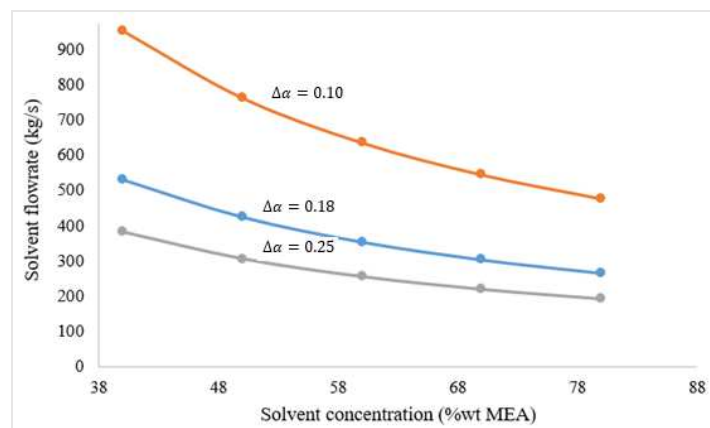
Fig.18 Solvent flowrate for different conditions

Typical stationary heat exchanger design such as the shell and tube and plate heat exchanger design are assesed here for the intercooler to determine heat exchange area needed for each case. For the purpose of this design, it has been assumed that the solvent temperature rises to about 343 K in the first RPB absorber before the intercooler (this is based on temperature rise expectations as demonstrated in Section 2) and the solvent is required to be cooled down to

26

about 313 K in the intercooler. Based on this assumption, the intercooler duty (Q) is estimated as follows:

$$Q = \dot{m}_{sol} \, C_{p,soln} \left(T_{sol,IN} - T_{sol,OUT} \right) \tag{19}$$

Cooling water is obtained based on energy balance, assuming the cooling water inlet and outlet temperature to be 288 K and 308 K respectively. Calculated duty and cooling water demand are given in Fig. 20. The result both show that cooling duty and cooling water requirement is less for the concentrated MEA solvent. This is because the sensible heat requirement is generally less due to the lower solvent flowrate (Fig. 18) and lower specific heat capacity (Table 1) of the concentrated MEA solvent.
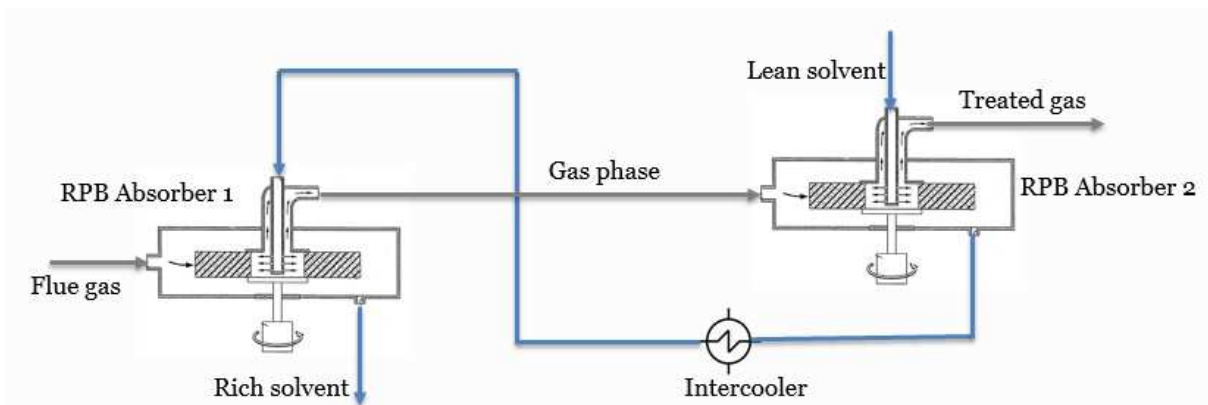

Fig. 19 RPB absorber setup with stationary intercooler

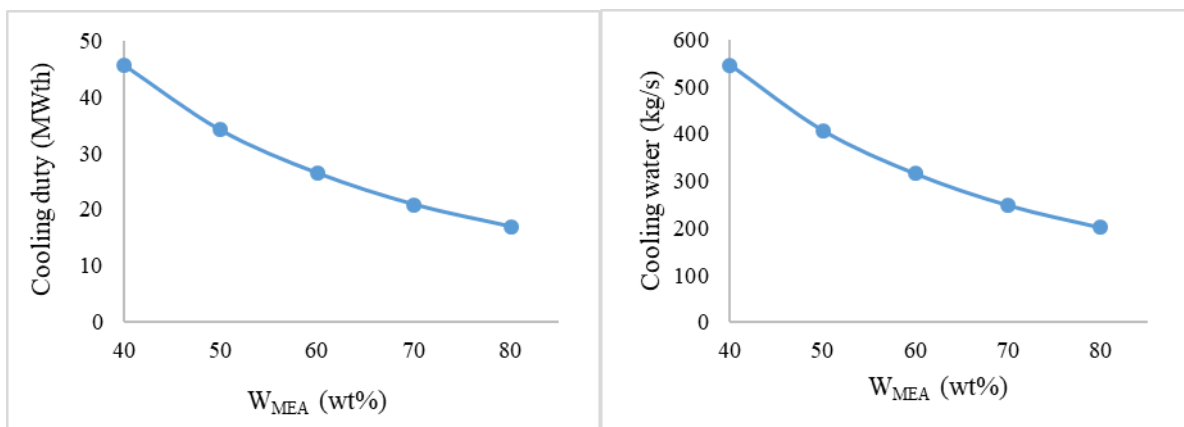Fig. 20. Cooling duty and cooling water

The heat exchanger area (A) is calculated as follows:

The short version of the paper was presented at ICAE2017, Aug 21-24, Cardiff, UK. This paper is a substantial extension of the short version of the conference paper.

$$A = \frac{Q}{UF_t \Delta T_{lm}}$$ (20)

For the shell and tube design, the overall heat transfer coefficient and the pressure drop is determined using standard procedures outlined in Sinnot [58] with the following assumptions:

- Stainless steel tubes of ¾ inch OD (by 16 ft length) desired due to the expected high level of corrosion.
- Triangular pitch tube arrangement
- The shell-bundle clearance (SBC) is obtained from design charts [58] with split ring floating exchanger (TEMA standard) assumed.

The ΔT_{lm} correction factor (F_t) for the shell and tube design is obtained as follows [58]:

$$F_t = \frac{\sqrt{(R_t^2 + 1)} \ln\left[\frac{1 - S_t}{1 - R_t S_t}\right]}{(R_t - 1) \ln\left[\frac{2 - S_t\left[R_t + 1 - \sqrt{(R_t^2 + 1)}\right]}{2 - S_t\left[R_t + 1 + \sqrt{(R_t^2 + 1)}\right]}\right]}$$ (21)

Where

$$R_t = \frac{T_{sol,IN} - T_{sol,OUT}}{T_{CW,OUT} - T_{CW,IN}}$$ (22)

$$S_t = \frac{T_{CW,OUT} - T_{CW,IN}}{T_{sol,IN} - T_{CW,IN}}$$ (23)

For the plate heat exchanger case, it must be noted first that they are generally suitable for viscous fluids such as the strong MEA solutions as they are able to achieve turbulence at much lower Reynolds Number, about 100-400 [58]. For this exchanger, the overall heat transfer coefficient is obtained from design chart [59] and the ΔT_{lm} correction factor F_t obtained from design charts in Sinnot [58]. The tube side pressure drop is estimated as follows [58]:

28

$$\Delta P = 4.8 Re^{-0.3} \left(\frac{L_p}{d_e}\right)\frac{\rho u_p^2}{2} \tag{24}$$

4.2.2 Rotary intercooler design

The stationary intercoolers described above involve large equipment, particularly in the case of the shell and tube heat exchangers. Also, with the stationary intercoolers between each RPB absorber, they could still be significant temperature excursions in the absorbers which will adversely affect the absorption performance. These considerations led to an alternative design approach in which the heat exchanger is incorporated within the rotating absorber, so that maximum benefit may be extracted from the enhanced acceleration environment.

The proposed design is outlined in Fig. 21. It can be seen that the cooling water stream is supplied to the rotor in narrow (~ 5 mm) channels which interleave with the absorption channels, within which the flue gas and MEA solution may flow co or counter-currently over the metallic foam packing. The MEA solution is assumed to flow radially outwards as a thin film over the reticulated foam packing under the prevailing centrifugal acceleration. Although some heat transfer benefit can be expected from the enhanced surface area represented by the "fin" effect of the packing, this has been ignored in the calculations below in order to provide a conservative performance estimate. Therefore, only the disc area is assumed to take part in the heat transfer process.

In contrast to the absorber channels, the cooling water channels will run full and will interleave with the absorber channels using porting arrangements which are qualitatively similar to those used in plate heat exchangers. This design approach ensures that the heat of absorption is removed as it is generated within the packing, thereby ensuring an optimum absorption environment at the lowest feasible temperature. The additional benefit is that this is achieved with only a marginal increase in equipment size. This is due to the relatively thin liquid film which can be generated in the enhanced acceleration environment, despite the viscosity of strong MEA solutions. The heat transfer performance and area requirement of the proposed arrangement is estimated as follows, subject to reasonable assumptions regarding the anticipated rotor structure.
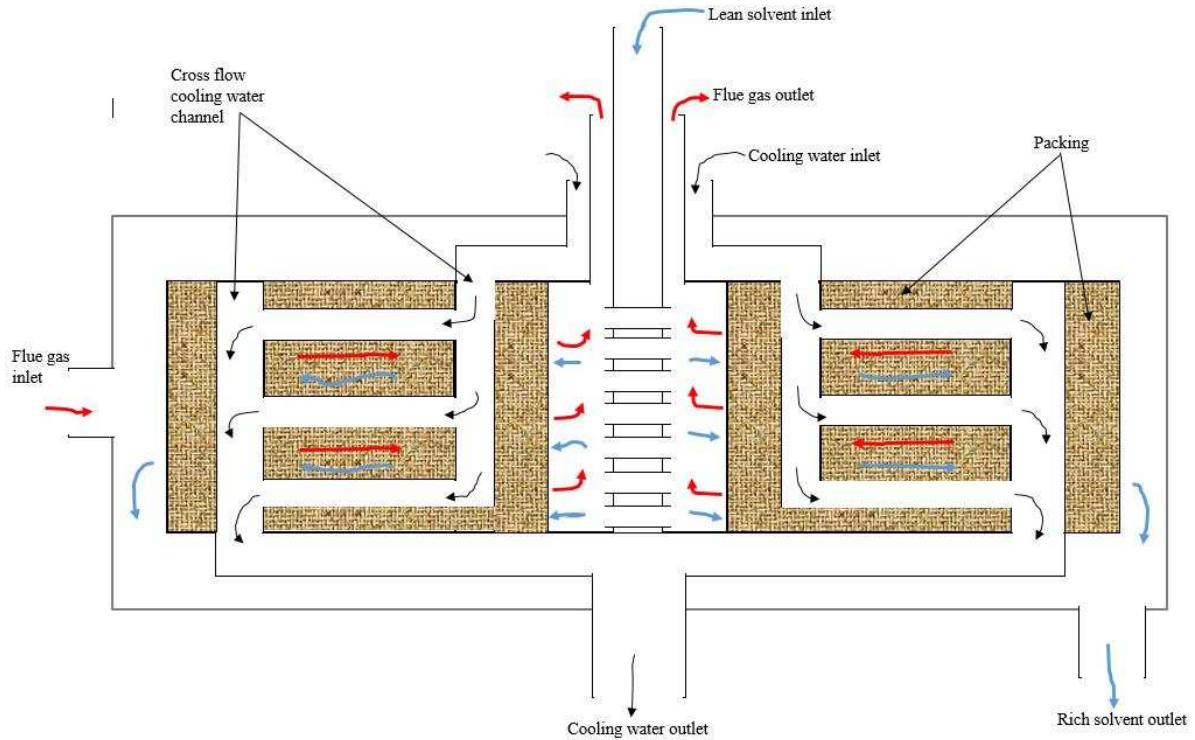
Fig. 21 New RPB absorber design with intercoolers

Available information is very limited and as a result we have made some assumptions (guided by the experience of Prof Colin Ramshaw, a renowned expert in this field) to obtain a rough estimate for the heat transfer area that will be needed to achieve similar ΔT_{lm} as in Section 4.2.1. On this basis, expected cooling duty and cooling water flowrate are therefore the same as in Section 4.1. From consideration of mass transfer and flooding data for RPB absorber [18], the RPB absorber for handling flue gas from a 250 MWe NGCC power plant is predicted to have packing diameter of about 6 m. A plate (or disc) thickness of 0.75 mm is assumed. Consequently, the heat transfer coefficient for the solvent side (h_{sol}) is based on the liquid film and is obtained as follows:

$$h_{sol} = \frac{k}{s} \tag{25}$$

Where:

k = thermal conductivity of the solution

s = liquid film thickness on the plate (or disc)

30

The short version of the paper was presented at ICAE2017, Aug 21-24, Cardiff, UK. This paper is a substantial extension of the short version of the conference paper.

The liquid film thickness is obtained as follows [60]:

$$s = \left(\frac{3\mu m}{2\pi \rho^2 w^2 r^2}\right)^{\left(\frac{1}{3}\right)} \tag{26}$$

Where:

w = rotational speed

r = radius

m = mass flowrate/disc

The heat transfer coefficient for the cooling water side is based on a standard correlation for plate heat exchangers given in Eqn 19 [61].

$$\frac{h_w d_e}{k_f} = 3.66 + \frac{0.0668\left[\left(\frac{L_p}{d_e}\right)/RePr\right]^{-1}}{1 + 0.04\left[\left(\frac{L_p}{d_e}\right)/RePr\right]^{-2/3}} \tag{27}$$

5 Results and discussions

5.1 Stationary intercooler

The heat transfer area and pressure drop for both shell and tube and plate heat exchanger designs have been evaluated to understand how both parameters are affected by MEA concentration. Comparing the heat transfer area for both designs in Figs. 22 and 23 showed that the plate heat exchanger designs will be about 10 times smaller than their shell and tube counterpart (in terms of heat transfer area) although in reality the actual area for the plate exchanger will be slightly larger than the estimated value to accommodate the ports and gasket area. The much reduced heat transfer area of the plate heat exchanger design is because of the lower heat transfer resistance as reflected in its higher overall heat transfer coefficients compared to the shell and tube heat exchanger design. The heat transfer area also decreases as MEA concentration increase for both designs. However, heat transfer becomes more inefficient at higher concentration as can be seen in the lower overall heat transfer coefficients. This is due to the higher viscosity of the solvent at higher concentration. The

lower heat transfer area at higher MEA concentration is driven not by the heat transfer efficiency but by the much reduced solvent flowrate at the concentration.

In terms of physical sizes, the plate heat exchanger will also be significantly smaller in volume compared to the shell and tube heat exchanger. To demonstrate this, a rough estimate of the volume of both exchangers were obtained for different solvent concentrations (Figs 24 and 25). For the shell and tube heat exchanger, it is assumed to be completely cylindrical with diameter equivalent to the shell diameter and the length obtained based on the tube length. The plate exchanger on the other hand is based on typical plate dimensions of 1.5 m x 0.5 m x 0.00075 m [54]. The estimate shows that in terms of physical size, that the plate exchanger will be up to 10-15 times smaller than the tubular exchanger depending on the solvent concentration.
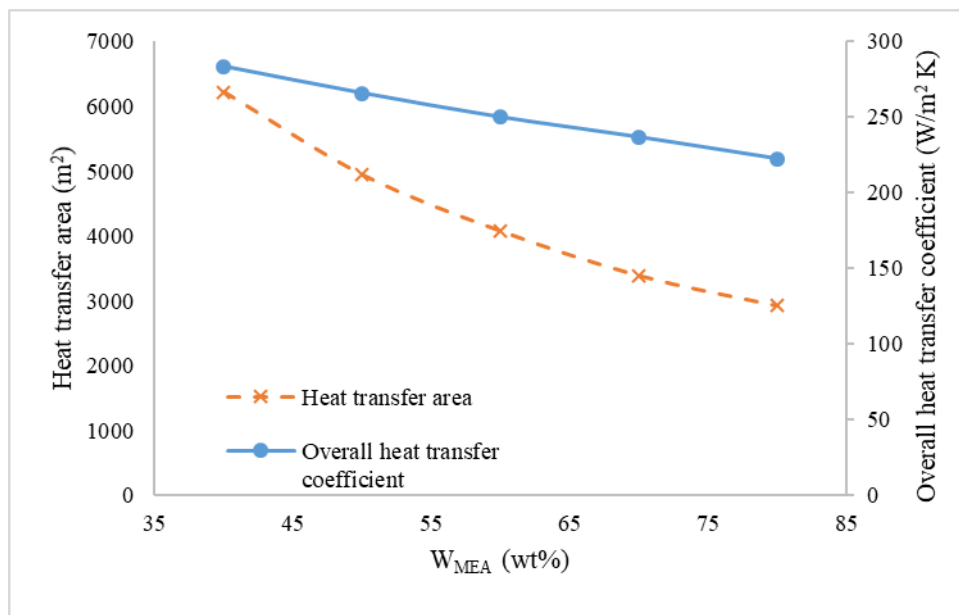
Fig. 22 Heat transfer area and overall heat transfer coefficient for shell and tube heat exchanger
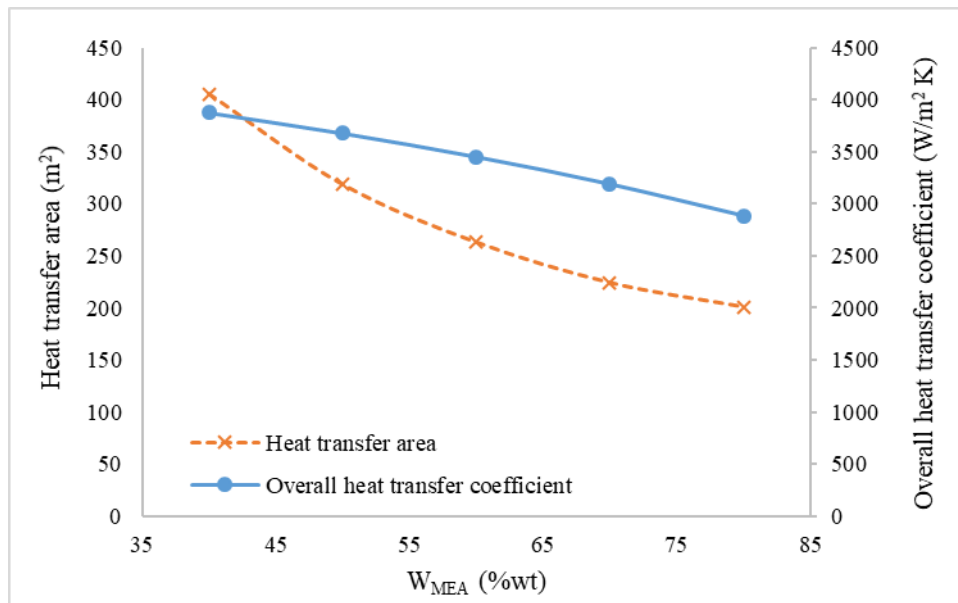
Fig. 23 Heat transfer area and overall heat transfer coefficient for plate heat exchanger

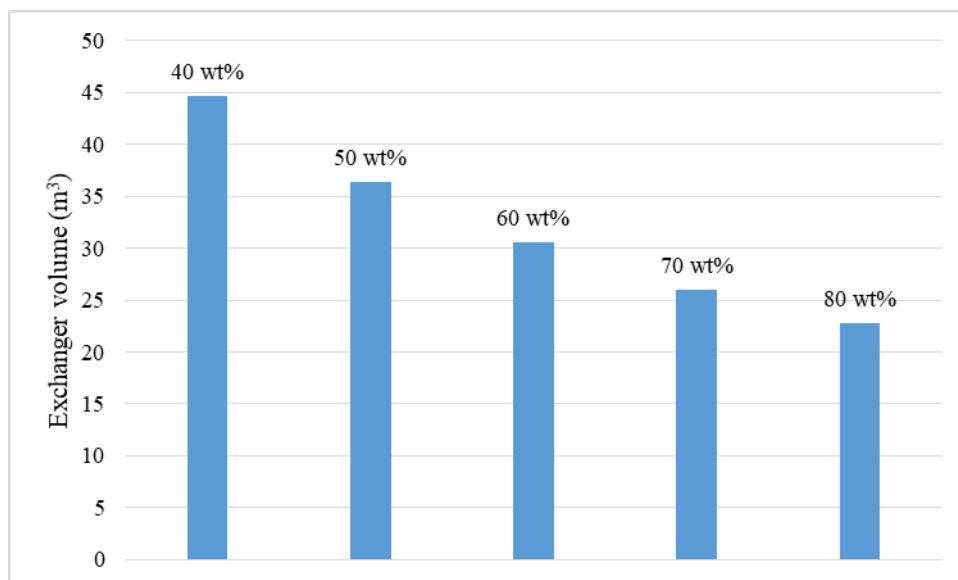Fig. 24 Estimates of shell-and-tube exchanger volume

Comparing the pressure drops, Figs 26 and 27, show that the pressure drop for plate exchanger is significantly higher and this gets worse as the solvent concentration increases. Although the plate exchanger design option offers an opportunity for more compact intercooler for the RPB absorber, the accompanying pressure drop is significantly higher.
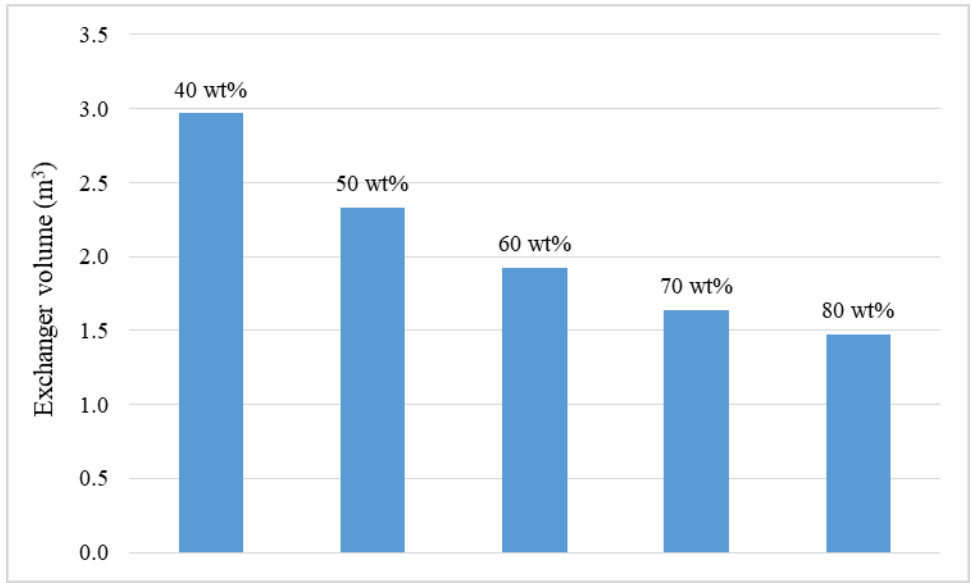
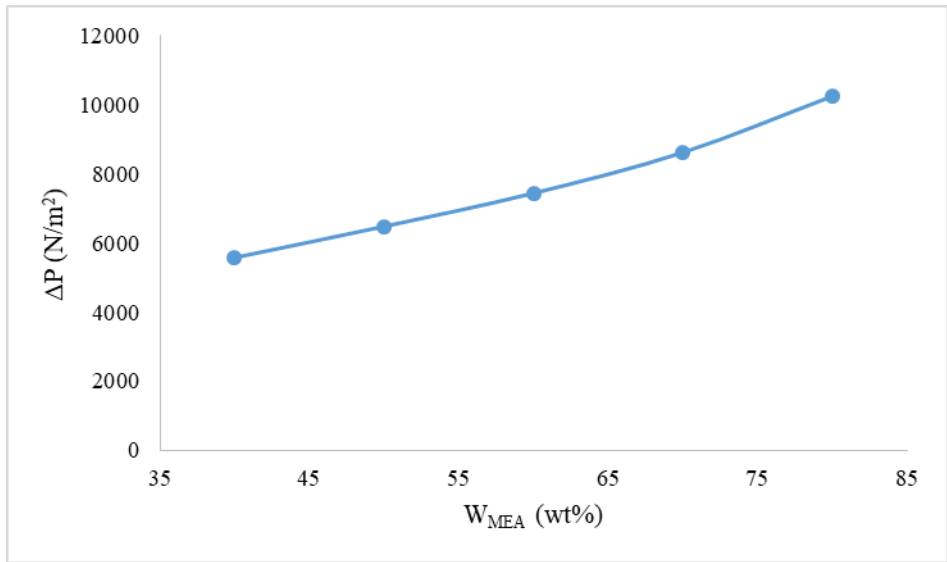Fig. 25 Estimates of plate heat exchanger volume

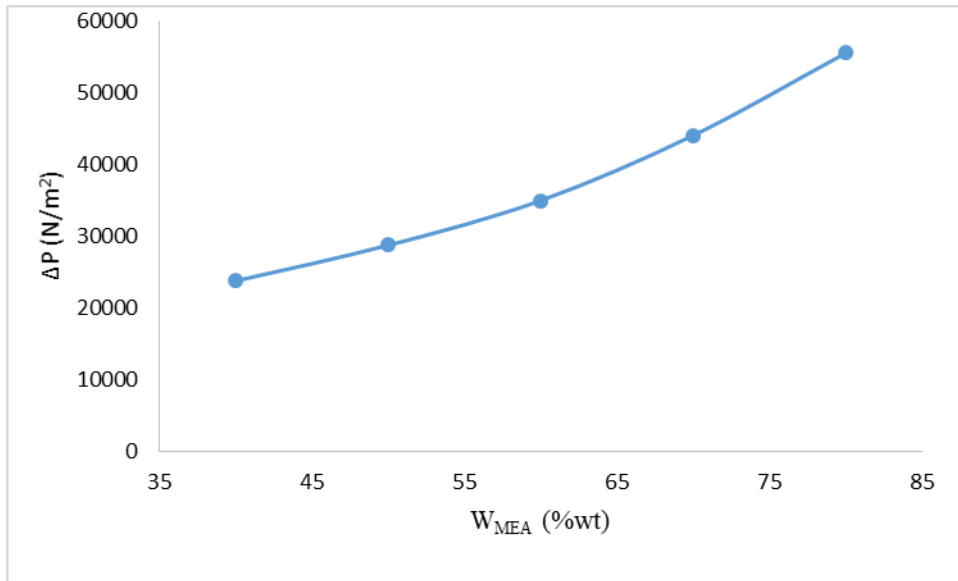Fig. 26 Pressure drop for shell and tube heat exchanger

Fig. 27 Pressure drop for plate exchanger design

5.2 Rotary intercooler

From the result in Fig 28, it is seen that the required heat transfer area is in similar range as the plate exchanger design but without pressure drop issues related to the intercooler. Analysis of the impact of the rotational speed (Fig 29) also showed that overall heat transfer resistance decreases significantly as the rotational speed increases. This will lead to smaller heat transfer area (Fig 29). The packings on the solvent side could also act as "fins" and further enhance heat transfer. As a result, the actual heat transfer area maybe significantly less than estimated values in this study. It must be stated that although this technique will bring benefits such as smaller heat transfer area, no pressure drop issues related to intercooler (as with the stationary intercoolers) and better absorption performance, that the axial height of the RPB will be slightly more. In this study, number of plates (=50) each of 0.75 mm thickness and 5 mm spacing have been assumed. This means that the axial height of the RPB will be increasing by about 0.2875 m. For an initial axial height of 2 m, this would represent an increase in axial height of about 14%. Also, the load on the rotating shaft will be more and the power consumption of the electrical motor will be slightly more. Regardless, the design will have far less footprint than the case involving plate exchanger design.
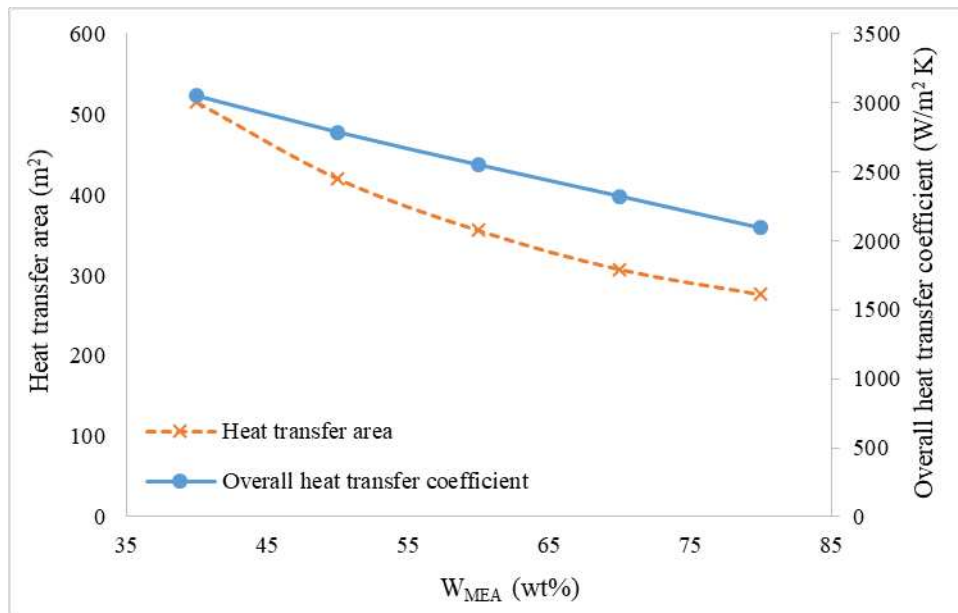
Fig. 28 New RPB absorber design with intercoolers at 500 RPM
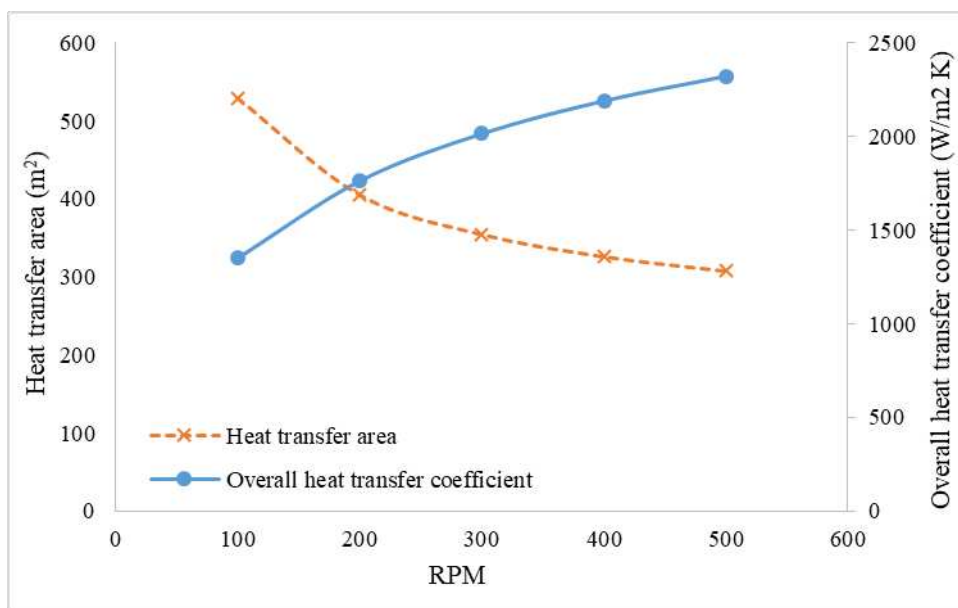
Fig. 29 New RPB absorber design at 70 wt% MEA concentration

6 Conclusions

In this study, the need for RPB absorber intercooler was demonstrated. This was done through energy balance calculations to determine the potential temperature rise for CO_2 absorption in different MEA concentrations. This was further analysed by evaluating the impact of temperature on the liquid phase composition, equilibrium partial pressure and the

The short version of the paper was presented at ICAE2017, Aug 21-24, Cardiff, UK. This paper is a substantial extension of the short version of the conference paper.

mass transfer resistance using a validated RPB absorber model implemented in gPROMS ModelBuilder®. The analysis showed that the liquid phase temperature will rise significantly and that the absorption rate could be affected significantly above 340 K temperature. Different RPB absorber intercooler designs - stationary and rotary designs - were introduced. The intercooler sizes and the associated pressure drops were estimated for scenarios involving different MEA concentrations as solvent using a benchmark flue gas flowrate from a 250 MWe NGCC power plant. From the estimates, the shell-and-tube designs will be bulky and negate the objective of reducing footprint with RPBs. The plate designs on the other hand are more compact, about 10 times smaller than the shell-and-tube designs but their pressure drop is higher. A rotary intercooler design is also proposed in this study which involves incorporating the intercooler in the RPB rotor. Initial estimates show that the required heat transfer area for this new design will be in the same range as that of the plate exchanger design.

Acknowledgements

References

[1] World Energy Council (WEC), 2016. Carbon Capture & Storage Available at: https://www.worldenergy.org/wp-content/uploads/2017/03/WEResources_CCS_2016.pdf [Accessed July, 2017]

[2] IPCC, 2014: Climate Change 2014: Synthesis Report. Contribution of Working Groups I, II and III to the Fifth Assessment Report of the Intergovernmental Panel on Climate Change [Core Writing Team, R.K. Pachauri and L.A. Meyer (eds.)]. IPCC, Geneva, Switzerland.

[3] Agrawal, N., Ahiduzzaman, Md. and Kumar, A. The development of an integrated model for the assessment of water and GHG footprints for the power generation sector. Applied Energy Vol. 216 (2018), 558-575.

[4] Oko, E., Wang, M. and Joel, A. S. Current status and future development of solvent-based carbon capture. Int. J. Coal Sci. Technol. Vol. 4 (2017), 5-14.

[5] Wang, M., Lawal, A., Stephenson, P., Sidders, J., & Ramshaw, C. (2011). Post-combustion CO_2 capture with chemical absorption: A state-of-the-art review. Chemical Engineering Research and Design, Vol. 89 (9), 1609–1624.

The short version of the paper was presented at ICAE2017, Aug 21-24, Cardiff, UK. This paper is a substantial extension of the short version of the conference paper.

[6] Diego, M. E., Bellas, J.-M. and Pourkashanian, M. Techno-economic analysis of a hybrid CO_2 capture system for natural gas combined cycles with selective exhaust gas recirculation. Applied Energy Vol. 215 (2018), 778-791.

[7] Oh, S.-Y., Yun, S. and Kim, J.-K. Process integration and design for maximizing energy efficiency of a coal-fired power plant integrated with amine-based CO_2 capture process. Applied Energy Vol. 216 (2018), 311–322.

[8] Wang, M., Joel, A.S., Ramshaw, C., Eimer, D. and Musa, N. M. Process intensification for post-combustion CO_2 capture with chemical absorption: A critical review. Applied Energy, 158 (2015), 275–291.

[9] Joel, A. S., Wang, M., Ramshaw, C., Oko, E. Process analysis of intensified absorber for post-combustion CO_2 capture through modelling and simulation. Journal of Greenhouse Gas Control, 21 (2014), 91–100.

[10] Kang, J.-L., Sun, K., Wong, D. S.-H., Jang, S.-S, and Tan, C.-S. Modelling studies on absorption of CO_2 by monoethanolamine in rotating packed bed. International Journal of Greenhouse Gas Control, 25 (2014), 141–150.

[11] Thiels, M., Wong, D. S. H., Yu, C.-H., Kang, J.-L., Jang, S. S., Tan, C.-S. (2016). Modelling and design of carbon dioxide absorption in rotating packed bed and packed column. In 11th IFAC Symposium on Dynamics and Control of Process Systems, including Biosystems. Trondheim, Norway.

[12] Joel, A. S., Wang, M., Ramshaw, C., Oko, E. Modelling, simulation and analysis of intensified regenerator for solvent based carbon capture using rotating packed bed technology. Applied Energy Vol. 203 (2017), 11–25

[13] HIGEE, 2014. Available at: http://higeeusa.com/Higee%20USA%20brochure.pdf [Accessed July, 2017]

[14] Oko, E., Wang, M. and Ramshaw, C. Study of mass transfer correlationsn for intensified absorbers in post-combustion CO_2 capture based on chemical absorption. 13th International Conference on Greenhouse Gas Control Technologies, GHGT-13, 14-18 Nov., 2016, Lausanne, Switzerland.

[15] Luo, Y., Chu, G.-W., Zou, H.-K., Wang, F., Xiang, Y., Shao, L. and Chen, J.-F. Mass transfer studies in a rotating packed bed with novel rotors: Chemisorption of CO_2. Ind. Eng. Chem. Res., 51 (2012), 9164−9172.

[16] Rao, D. P., Bhowal, A. and Goswami, P. S. Process intensification in rotating packed beds (HIGEE): An appraisal. Ind. Eng. Chem. Res, 43 (2004), 1150–1162.

[17] Luo, Y., Chu, G.W., Zou, H.K. Zhao, Z.Q., Dudukovic, M.P. and Chen, J. F. (2012). Gas−liquid effective interfacial area in a rotating packed bed. Ind. Eng. Chem. Res., 51, 16320−16325.

[18] Jassim, M.S., Rochelle, G., Eimer, D., Ramshaw, C. (2007). Carbon dioxide absorption and desorption in aqueous monoethanolamine solutions in a rotating packed bed. Industrial & Engineering Chemistry Research, 46(9), 2823–2833.

[19] Chen, Y. S.; Liu, H. S. (2002). Absorption of VOCs in a rotating packed bed. Ind. Eng. Chem. Res., 41, 1583

[20] Llerena-Chavez, H. and Larachi, F. 2009. Analysis of flow in rotating packed beds via CFD simulations—Dry pressure drop and gas flow maldistribution. Chemical Engineering Science, 64, 2113-2126.

[21] Freguia, S and Rochelle, G. T. (2003). Modeling of CO_2 capture by aqueous monoethanolamine. AIChE Journal, 49(7), 1676–1686.

[22] Kvamsdal, H.M. and Rochelle, G.T. Effects of the temperature bulge in CO_2 absorption from flue gas by aqueous monoethanolamine. Ind. Eng. Chem. Res. 47 (2008), 867-875.

[23] Biliyok, C., Lawal, A., Wang, M. and Seibert, F. Dynamic modelling, validation and analysis of post-combustion chemical absorption CO_2 capture plant. International Journal of Greenhouse Gas Control Vol. 9 (2012), 428–445.

[24] Oko, E., Wang, M. and Joel, A. S. Current status and future development of solvent-based carbon capture. International Journal of Coal Science & Technology 2017, Vol. 4 (1), 5-14.

[25] Chambers, H.H. and Wall, R.G. Some factors affecting the design of centrifugal gas absorbers. Trans. Instn Chem. Engrs. 32 (1954), 96-107.

[26] Kittel, J., Idem, R., Gelowitz, D., Tontiwachwuthikul, P., Parrain, G. and Bonneau, A. Corrosion in MEA units for CO_2 capture: pilot plant studies. Energy Procedia 1 (2009), 791-797

[27] Ying, J. and Eimer, D. A. (2013). Determination and measurements of mass transfer kinetics of CO_2 in concentrated aqueous monoethanolamine solutions by a stirred cell. Ind. Eng. Chem. Res., 52(7), 2548–2559.

[28] Oexmann, V. J (2011). Post-combustion CO_2 capture: Energetic evaluation of chemical absorption processes in coal-fired steam power plants. PhD Thesis Technical University of Hamburg, Germany.

[29] Cousins, A., Cottrell, A., Lawson, A., Huang, S. and Feron, P.H.M. Model verification and evaluation of the rich-split process modification at an Australian-based post combustion CO_2 capture pilot plant. Greenhouse Gas Sci Technol. Vol. 2, (2012), 329–345.

[30] Joel, A.S. 2016. Study of process intensification for post-combustion carbon capture based on chemical absorption through modelling and simulation. PhD Thesis, University of Hull, UK.

[31] Agbonghae, E.O, Hughes, K.J, Ingham, D.B, Ma, L., Pourkashanian, M. Optimal process design of commercial-scale amine-based CO_2 capture plants. Ind. Eng. Chem. Res Vol. 53 (2014), 14815-29.

[32] Yu, C.-H., Cheng, H.-H. and, & Tan, C.-S. CO_2 capture by alkanolamine solutions containing diethylenetriamine and piperazine in a rotating packed bed. International Journal of Greenhouse Gas Control, 9 (2012), 136–147.

[33] Eni Oko, Colin Ramshaw, Meihong Wang. Study of absorber intercooling in solvent-based CO_2 capture based on rotating packed bed technology. Energy Procedia 142 (2017) 3511–3516.

[34] Jou, F.-Y., Otto, F. D. and Mather, A. E. (1994). Vapor-liquid equilibrium of carbon dioxide in aqueous mixtures of monoethanolamine and methyldiethanolamine. Ind. Eng. Chem. Res., 33, 2002–2005.

[35] Kim, I., Hoff, K. A. and Mejdell, T. (2014). Heat of absorption of CO_2 with aqueous

The short version of the paper was presented at ICAE2017, Aug 21-24, Cardiff, UK. This paper is a substantial extension of the short version of the conference paper.

solutions of MEA: new experimental data. Energy Procedia, 63, 1446 – 1455.

[36] Aronu, U.E., Gondal, S., Hessen, E.T., Haug-Warberg, T., Hartono, A., Hoff, K.A. and Svendsen, H. F. (2011). Solubility of CO_2 in 15, 30, 45 and 60 mass% MEA from 40 to 120 °C and model representation using the extended UNIQUAC framework. Chemical Engineering Science, 66, 6393–6406.

[37] Mason, J.W. and Dodge, B. F. (1936). Equilibrium absorption of carbon dioxide by solutions of the ethanolamines. Trans. Am. Inst. Chem. Eng., 32, 27–48.

[38] Mathonat, C., Majer, V., Mather, A. and Grolier, J.-P. (1998). Use of flow calorimetry for determining enthalpies of absorption and the solubility of CO_2 in aqueous monoethanolamine solutions. Industrial & Engineering Chemistry Research, 37, 4136–4141.

[39] Lee, J. I., Otto, F. D., Mather, A. E. (1974). The solubility of H_2S and CO_2 in aqueous monoethanolamine solutions. Can. J. Chem. Eng., Vol. 52 (6), 803-805.

[40] Aboudheir, A., Tontiwachwuthikul, P., Chakma, A. and Idem, R. Kinetics of the reactive absorption of carbon dioxide in high CO_2-loaded, concentrated aqueous monoethanolamine solutions. Chemical Engineering Science 2003, 58, 5195-5210.

[41] Rackett, H.G. Equation of state   J. Chem. Eng. Data., Vol. 15, Issue 4, (1970), 514-517.

[42] Jayarathna, S. A., Weerasooriya, A., Dayarathna, S., Eimer, D. A. and Melaaen, M. C. Densities and surface tensions of CO_2 loaded aqueous monoethanolamine solutions with r = (0.2 to 0.7) at T = (303.15 to 333.15) K. J. Chem. Eng. Data 2013, 58, 986−992

[43] Horvath, A. L. Handbook of Aqueous Electrolyte Solutions. Chichester: Ellis Horwood, 1985.

[44] Amundsen, T. G., Øi, L. E. and Eimer, D. A. Density and Viscosity of Monoethanolamine + Water + Carbon Dioxide from (25 to 80) °C. J. Chem. Eng. Data 2009, 54, 3096−3100.

[45] Agbonghae, E.O., Hughes, K.J., Ingham, D.B., Ma, L. and Pourkashanian, M. A semi-empirical model for estimating the heat capacity of aqueous solutions of alkanolamines for CO_2 capture

[46] Ying, J. and Eimer, D.A. Measurement and correlations of diffusivities of nitrous oxide and carbon dioxide in monoethanolamine + water by laminar liquid jet. Ind. Eng. Chem. Res., **2012**, 51 (50), pp 16517–16524

[47] Ying, J., Eimer, D. A. and Yi, W. Measurements and correlation of physical solubility of carbon dioxide in (monoethanolamine + water) by a modified technique. Ind. Eng. Chem. Res., 2012, 51, 6958−6966.

[48] Knudsen, J. G., Hottel, S.M. H.C., Sarofim, A.F. & Wankat, P. C. and Knaebel, K.S., 1997. Heat and mass transfer. In D. W. Perry, Robert H., Green & J. O. and Maloney, eds. *Perry's Chemical Engineers' Handbook*, McGraw-Hill Education, New York.

[49] Kvamsdal, H.M., Jakobsen, J.P. and Hoff, K.A. Dynamic modelling and simulation of CO_2 absorber column for post-combustion CO_2 capture. Chemical Engineering and Processing 2009, 48(1), 135–144.

[50] Billets, R. and Schultes, M. Prediction of mass transfer columns with dumped and arranged packings: Updated summary of the calculation method of Billet and Schultes. Trans

    The short version of the paper was presented at ICAE2017, Aug 21-24, Cardiff, UK. This paper is a substantial extension of the short version of the conference paper.

IChemE 1999, 77 Part A, 498–504.

[51] Tung, H. H.; Mah, R.S.H. Modeling liquid mass transfer in Higee separation process. Chem. Eng. Commun. 1985, **39**, 147-153

[52] Chen, Y.-S. Correlations of mass transfer coefficients in a rotating packed bed. Ind. Eng. Chem. Res. 2011, **50**, 1778–1785.

[53] Jassim, M.S. 2002. Process intensification: Absorption and desorption of carbon dioxide from monoethanolamine solutions using HIGEE technology. Ph.D. Thesis, University of Newcastle, UK.

[54] Austgen, D.M., Rochelle, G.T., Peng, X. and Chen, C.-C. Model of vapor-liquid. equilibria for aqueous acid gas-alkanolamine systems using the electrolyte-NRTL equation. Ind. Eng. Chem. Res., 28 (1989), 1060–1073

[55] Liu, Y., Zhang, L. and Watanasiri, S. Representing vapor-liquid equilibrium for an aqueous MEA-CO_2 system using the electrolyte non-random-two-liquid model. Ind. Eng. Chem. Res., 38 (1999), 2080–2090.

[56] Canepa, R., Wang, M., Biliyok, C. and Satta, A. 2012. Thermodynamic analysis of combined cycle gas turbine power plant with post-combustion CO_2 capture and exhaust gas recirculation. Proc. IMechE Part E: J Process Mechanical Engineering 227(2), 89–105.

[57] Lawal, A., Wang, M., Stephenson, P. and Obi, O. Demonstrating full-scale post-combustion CO_2 capture for coal-fired power plants through dynamic modelling and simulation. Fuel 101 (2012) 115–128.

[58] Sinnot, R. . (2005). *Coulson & Richardson's Chemical Engineering* (4th Ed.). Elsevier Butterworth-Heinemann.

[59] Haslego, C. and Polley, G. Compact Heat Exchangers - Part I: Designing plate-and-frame heat exchangers. CEP Magazine, Sept., 2002. Retrieved from http://www.mie.uth.gr/ekp_yliko/CEP_Plate_and_Frame_HX.pdf

[60] Butterworth, D. and G.F. Hewitt, 1977. Two Phase Flow and Heat Transfer, Oxford University Press, UK.

[61] Knudsen, J.G. and Katz, D.L. 1958. Fluid dynamics and heat transfer. McGraw-Hill Book Company, Inc., New York.